SLAC-PUB-2433
November 1979
(T/E)

QCD PHENOMENOLOGY OF THE LARGE p_T PROCESSES

R. Stroynowski

Stanford Linear Accelerator Center
Stanford University, Stanford, California 94305

Lectures

at

the

SLAC Summer Institute on Particle Physics:

Quantum Chromodynamics

at

Stanford, California

July 9 - 20, 1979

* Work supported by the Department of Energy under contract number DE-AC03-76SF00515.

TABLE OF CONTENTS

1. INTRODUCTION

In the early experiments at the ISR it was found that the transverse momentum spectrum of produced pions followed a steep exponential fall-off at low values of p_T. Such behaviour was expected from the extrapolation of the low energy data. It came therefore as a surprise that in three independent experiments[1-3] the invariant cross section distribution of charged pions was observed to deviate strongly from the e^{-6p_T} dependence at large p_T. This discovery coincided with the advent of the quark-parton model[4,5] in which hard scattering of point-like partons was expected to produce events with large p_T secondaries, and it raised hopes that in such processes one had started to probe the structure of hadronic reactions at very short distances. The fast paced activities which followed during the next few years produced a vast amount of data supporting the qualitative features of the parton picture. The quantitative description of the data required, however, sophisticated extensions of the parton model, e.g., quark fusion model, Constituent Interchange Model (CIM), etc. For the discussion of these models and the summary of the earlier data the reader is referred to other review.[6-8] Today the Quantum Chromodynamics (QCD) provides a framework for the possible high accuracy calculations of the large p_T processes. The QCD phenomenology is somewhat more complicated here than in the case of deep inelastic lepton scattering or the Drell-Yan mechanism; nevertheless, it appears to be quite successful.

In the first part of these lectures I will introduce the description of the large transverse momentum phenomena in terms of the parton model and describe the modifications expected from QCD using as an example

single particle distributions. In sections 4 to 7 I will review the present status of available data, the evidence for jets and the future prospects.

2. POINT-LIKE DESCRIPTION OF LARGE p_T PROCESSES

2.1 Definitions and Variables

The basic diagram of the hard scattering process is shown in Fig. 1. In such process constituent "a" carrying the fraction x_a of the parent particle A momentum interacts with the constituent "b" from the target. The resulting constituents "c" and "d" then fragment into the experimentally observable final state particles, i.e., mesons, baryons, etc. Among those particles there is a final state hadron h, which tags the event as having a large p_T secondary. This hadron h carries a fraction z of the parent constituent "c" momentum. In the approximation when transverse momentum and masses of the constituents insde the parent hadron may be neglected, the subprocess variables $\hat{s}$ and $\hat{t}$ may be related to the overall center of mass variables by:

$$\hat{s} = x_a x_b s \quad ,$$

$$\hat{t} = x_a t/s \quad ,$$

$$z = \frac{-1}{s}\left(\frac{t}{x_b} + \frac{u}{x_a}\right),$$

where t and u are defined as:

$$t = (p_A - p_h)^2 \quad ,$$

$$u = (p_B - p_h)^2 \quad .$$

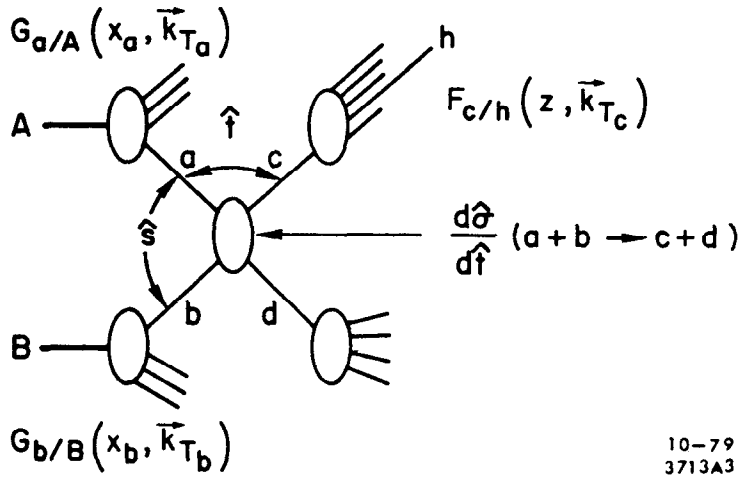

Fig. 1. A general diagram for hard scattering models of large p_T processes.

The general expression for the differential cross section distribution of the large p_T process is then given by:

$$E\frac{d^3\sigma}{dp^3} = \sum_{a,b}\int dx_a dx_b d^2k_{T_a} d^2k_{T_b} d^2k_{T_c} \cdot$$

$$G_{a/A}(x_a,\vec{k}_{T_a})G_{b/B}(x_b,\vec{k}_{T_b})\frac{1}{\pi}\frac{d\hat{\sigma}}{dt}(\hat{s},\hat{t})\frac{1}{z}F_{c/h}(z,\vec{k}_{T_c}). \qquad (1)$$

Here functions G represent the probability distributions of finding constituent a or b in parent particles A and B with corresponding fractions of their momenta x_a and x_b. Similarly, function F represents the probability that the constituent c will fragment into the hadron h with fraction z of the c momentum. Finally, $\frac{d\hat{\sigma}}{d\hat{t}}$ describes the cross section for the subprocess a + b → c + d.

2.2 Simple Parton Model

In 1971 Berman, Bjorken and Kogut calculated[4] the expectations for the hard scattering process following from the simple parton model. In this approach the constituents a, b, c, and d were assumed to be quarks and the point-like scattering subprocess was expected to proceed via the vector gluon exchange. The subprocess cross-section.

$$\frac{d\hat{\sigma}}{d\hat{t}} \sim \frac{1}{\hat{s}^2} \ ,$$

inserted into formula (1), resulted in the differential single particle distributions of the form:

$$E\frac{d^3\sigma}{dp^3} \sim p_T^{-n} f(x_T,\theta) \ , \qquad (2)$$

where $x_T=2p_T/\sqrt{s}$. The power of the p_T dependence, n=4, was in agreement with expectations from the dimensional arguments. The formula (2) reflected the scaling properties of the parton model, i.e., the function $f(x_T,\theta)$ depended only on the dimensionless quantities and was expected for large x_T to be of the form[9-11]:

$$f(x_T,\theta) \sim (1-x_T)^m \quad . \tag{3}$$

In addition, final state particles were expected to form four jets: two coming from the fragmentation of the scattered quarks and two from the spectator systems of the incoming hadrons.

The large amount of the experimental information collected during the following years at the ISR and in Fermilab showed rather surprising characteristics. The data confirmed most of the qualitative expectations of the simple parton model, i.e., approximate scaling (see Fig. 2), existence of jets, shape of the scaling function, etc. The single particle p_T distributions had, however, much steeper fall-off than expected: $n \sim 8$ for pions and kaons and $n \sim 10 \div 12$ for protons.

Within the framework of the parton model, two distinct classes of remedies of this problem were developed.

1. The "black box" model. Feynman, Field and Fox had proposed[12,13] that for some unknown reason the hard scattering subprocess violates the field theory expectations. Assuming arbitrarily $\frac{d\hat{\sigma}}{d\hat{t}} \sim \frac{1}{\hat{s}\hat{t}^3}$, which leads to p_T^{-8} dependence of the single particle distribution and introducing transverse momentum smearing, they have attained remarkable phenomenological success in describing available data while preserving the simplicity of the parton model.

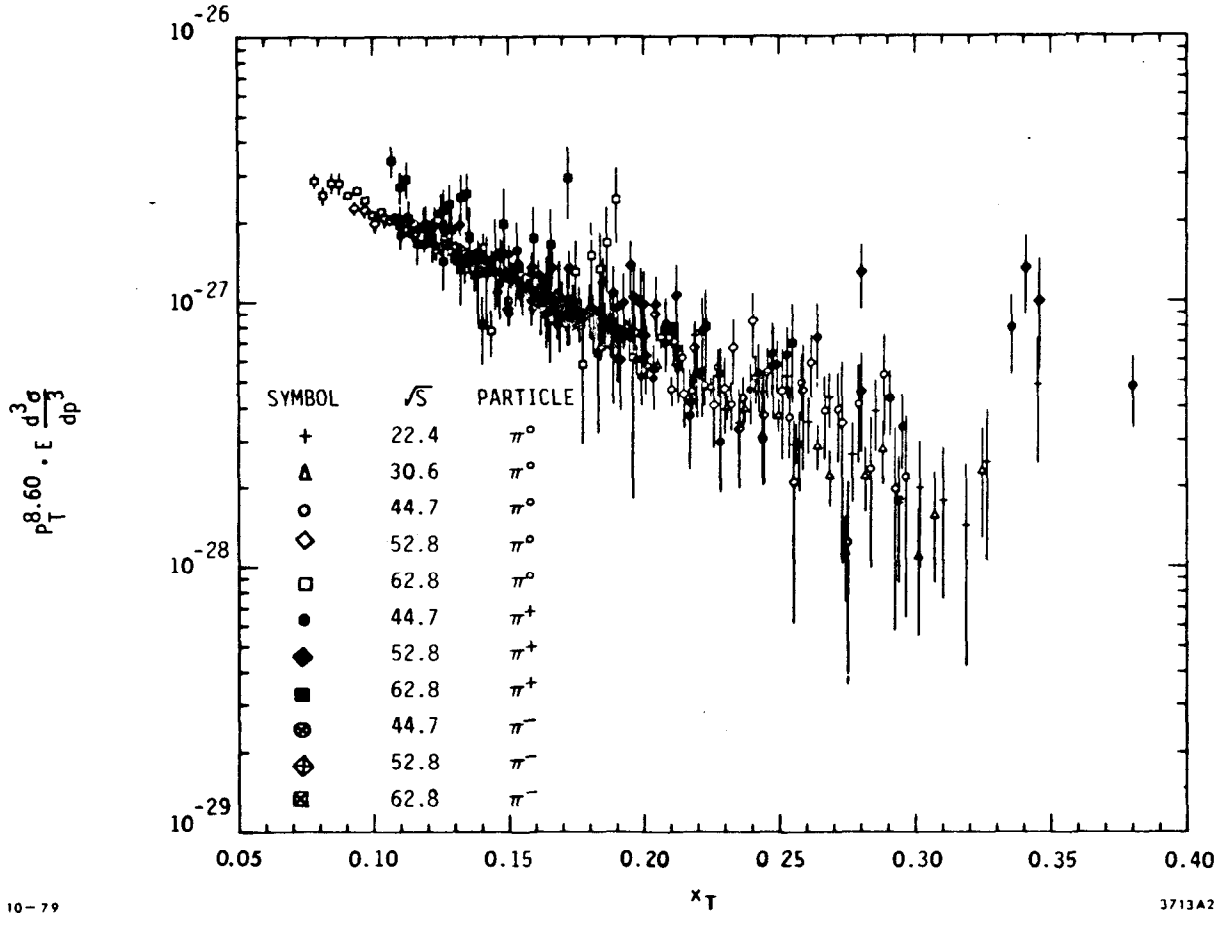

Fig. 2. Plot of the function $f(x_T,\theta)$ for π^+, π^- and π° (ref. 35).

2. The proponents of the Constituent Interchange Model (CIM)[14] and also the quark-fusion model[15] have argued that in addition to the quark-quark scattering there are also other subprocesses contributing to the data in the kinematical region of the available data. These are the quark-meson and quark-diquark scattering which include as the cross term also the quark fusion process (see Fig. 3). For such diagrams the dimensional counting rules predicted n=8 for pions and kaons and n=12 for baryons in good agreement with experimental measurements. The model introduced unknown coupling of quarks to mesons and unknown distributions of mesons inside the parent hadrons. Its application was rather complicated due to many possible diagrams contributing to the large p_T process. Nevertheless, it described most of the available data on single particle distributions and correlations.

More extensive discussion of the above models can be found in Reference 7. Both of the above approaches encountered difficulties in explaining certain aspects of correlations in large p_T events and recently were abandoned in favour of the systematic QCD calculations. Nevertheless, certain elements of these approaches are preserved also in the QCD phenomenology.

3. QCD DESCRIPTION OF LARGE p_T PROCESSES

3.1 Perturbative Approach

The arguments used in the discussion of the QCD description of large p_T events follow the same pattern as those for the Drell-Yan mechanism.[16] Here again possible emission of gluons modifies the parton model calculations. In the perturbative approach, it was shown[17] that in the leading

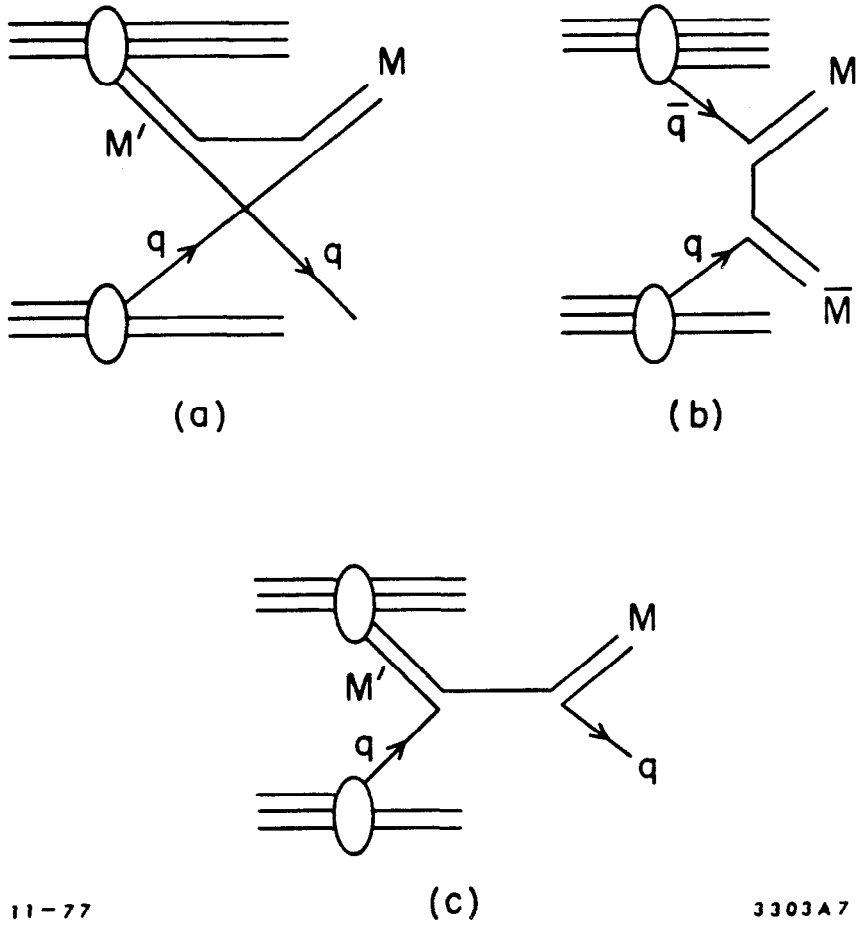

Fig. 3. The diagrams of the Constituent Interchange Model.

$\log Q^2$ approximation one can factorise the divergent parts ("mass singularity") of the contributions to the formula (1) due to the collinear gluon emission. These parts can then be incorporated into either distribution functions $G(x,Q^2)$ for finding quarks and gluons inside the parent particle or into the fragmentation functions $F(x,Q^2)$. These new so-called renormalisation-group-improved distribution functions are again the same as measured in deep inelastic lepton scattering experiments, while the fragmentation functions are the same as measured in the e^+e^- annihilation into hadrons. The procedure is graphically illustrated in Fig. 4. The large dimensional quantity Q^2, entering the scale breaking terms in the perturbative approach, is not uniquely defined for large p_T processes and will be discussed later.

There are eight elementary subprocesses which contribute to the leading power law behaviour; these are $qq \to qq$, $\bar{q}q \to \bar{q}q$, $\bar{q}\bar{q} \to \bar{q}\bar{q}$, $qg \to qg$, $\bar{q}g \to \bar{q}g$, $gg \to gg$, $gg \to q\bar{q}$ and $q\bar{q} \to gg$. Their cross section distributions have the general form

$$\frac{d\hat{\sigma}}{d\hat{t}} = \pi\alpha_s^2(Q^2)\,\frac{|A|^2}{\hat{s}^2} \quad , \tag{4}$$

where $|A|^2$ have been calculated[18] for all first order in α_s diagrams and are listed in Table I.

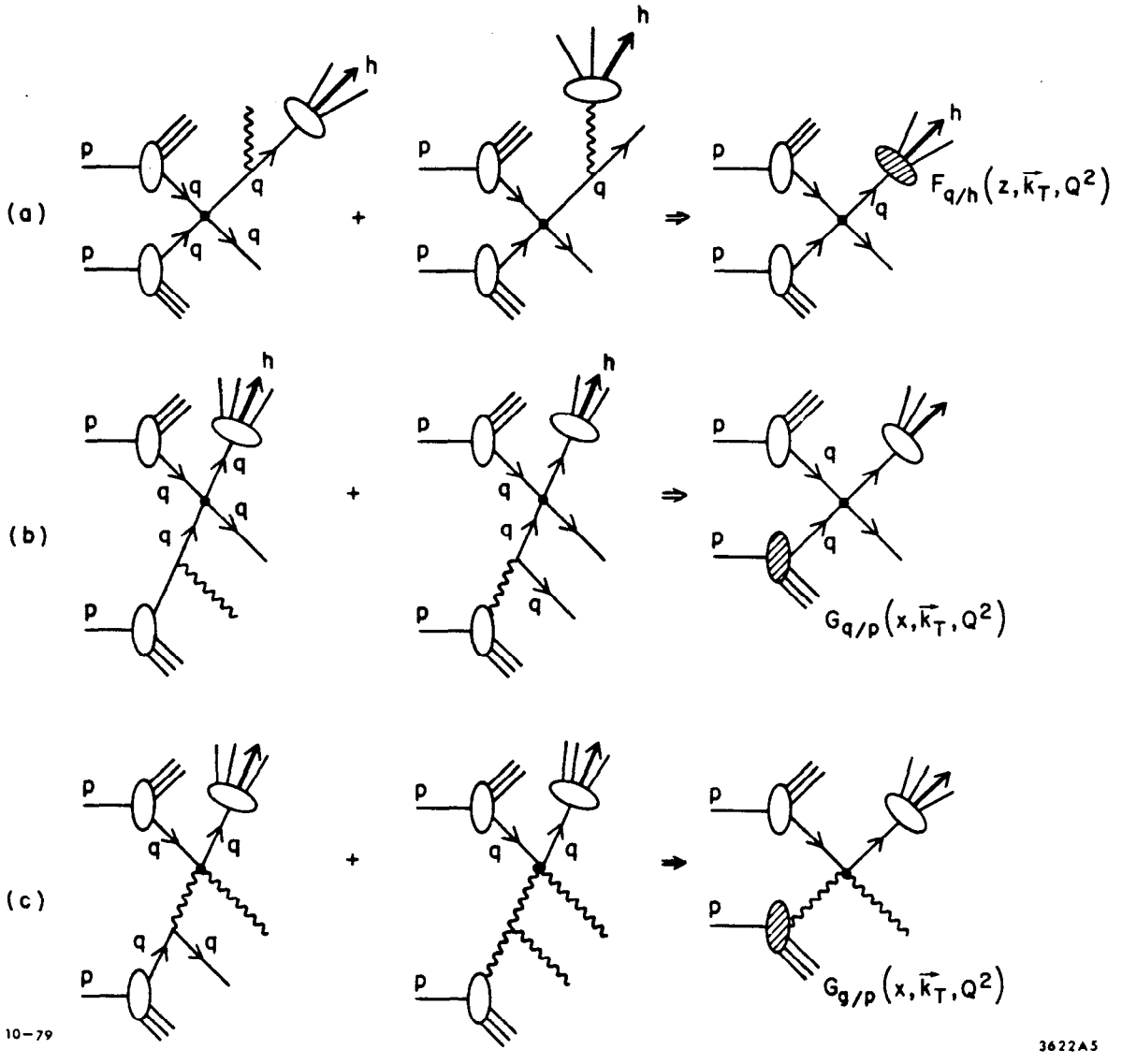

Fig. 4. Illustration of the diagrams contributing to the renormalisation-group-improved a) fragmentation function, b) quark distribution function and c) gluon distribution function.

TABLE I

Subprocess	$\lvert A\rvert^2$
$q_i q_j \to q_i q_j$, $q_i \bar{q}_j \to q_i \bar{q}_j$ $\left.\right\} i \neq j$	$\frac{4}{9}\,\frac{\hat{s}^2+\hat{u}^2}{\hat{t}^2}$
$q_i q_i \to q_i q_i$	$\frac{4}{9}\left(\frac{\hat{s}^2+\hat{u}^2}{\hat{t}^2}+\frac{\hat{t}^2+\hat{s}^2}{\hat{u}^2}\right)-\frac{8}{27}\,\frac{\hat{s}^2}{\hat{u}\hat{t}}$
$q_i \bar{q}_i \to q_i \bar{q}_i$	$\frac{4}{9}\left(\frac{\hat{s}^2+\hat{u}^2}{\hat{t}^2}+\frac{\hat{t}^2+\hat{u}^2}{\hat{s}^2}\right)-\frac{8}{27}\,\frac{\hat{u}^2}{\hat{s}\hat{t}}$
$q_i \bar{q}_i \to gg$	$\frac{32}{27}\,\frac{u^2+t^2}{\hat{u}\hat{t}}-\frac{8}{3}\,\frac{\hat{u}^2+\hat{t}^2}{\hat{s}^2}$
$gg \to q_i \bar{q}_i$	$\frac{1}{6}\,\frac{\hat{u}^2+\hat{t}^2}{\hat{u}\hat{t}}-\frac{3}{8}\,\frac{\hat{u}^2+\hat{t}^2}{\hat{s}^2}$
$q_i g \to q_i g$	$-\frac{4}{9}\,\frac{\hat{u}^2+\hat{s}^2}{\hat{u}\hat{s}}+\frac{\hat{u}^2+\hat{s}^2}{\hat{t}^2}$
$gg \to gg$	$\frac{9}{2}\left(3-\frac{\hat{u}\hat{t}}{\hat{s}^2}-\frac{\hat{u}\hat{s}}{\hat{t}^2}-\frac{\hat{s}\hat{t}}{\hat{u}^2}\right)$
$q_i \bar{q}_i \to q_j \bar{q}_j$	$\frac{4}{9}\,\frac{\hat{t}^2+\hat{u}^2}{\hat{s}^2}$

3.2 QCD Phenomenology

The perturbative approach described in Section 3.1 results in the form of the differential cross section distributions analogous to Eq. (1):

$$E\frac{d^3\sigma}{dp^3}(s,p_T,\theta^*) = \sum_{a,b}\int dx_a dx_b$$

$$G_{a/A}(x_a,Q^2)G_{b/B}(x_b,Q^2)\frac{1}{\pi}\frac{d\hat{\sigma}}{d\hat{t}}(a+b\to c+d)\frac{1}{z}F_{c/h}(z,Q^2) \quad . \quad (5)$$

The scaling, predicted in the parton model, is now violated following the pattern of the scale breaking of the distribution and fragmentation functions. Here, however, in contrast with the Drell-Yan mechanism, the convolution of the three components, each with its own pattern of scale violation, prevents the formulation of the intuitive predictions for the qualitative behaviour of the single particle distribution.

There are several recently published papers[19-24] with the phenomenological applications of Eq. (5) to the data on large p_T processes. In general they follow similar prescriptions, varying in particular choices for certain ingredients. As an example I will list the elements of calculations chosen by Feynman, Field and Fox.[19]

1. Strong coupling constant. The general form

$$\alpha_s(Q^2) = \frac{12\pi}{(33-2n_f)\ln Q^2/\Lambda}$$

is usually reduced by choosing the number of flavours $n_f = 4$. Although the parameter Λ defining the scale of the perturbative calculations may, in principle, be process dependent, it is usually determined in the analysis of deep inelastic lepton scattering data and in most of the phenomenological applications it is set[25] to $\Lambda = 0.4$.

2. Scale breaking variable Q^2. The identification of the large, dimensional quantity Q^2 is not unique for the large p_T processes. The difficulty is introduced by the ambiguity between the s and t channels of the subprocess reaction $a + b \to c + d$. Feynman, Field and Fox[19] defined Q^2 as

$$Q^2 = \frac{2\hat{s}\hat{t}\hat{u}}{\hat{s}^2 + \hat{t}^2 + \hat{u}^2} \quad ,$$

while Combridge, Kripfganz and Ranft used[18]

$$Q^2 = \sqrt[3]{\hat{s}\hat{t}\hat{u}} \quad .$$

At very large transverse momentum of the triggering particle these choices are equivalent to the one used by Brodsky, Gunion and their collaborators:[22,23]

$$Q^2 = -\hat{t}.$$

At intermediate p_T, however, the various definitions may introduce[26] differences of up to 50%.

3. Cut-off procedure. The subprocess cross-sections listed in Table I are divergent for $\hat{s}$, $\hat{t}$, or $\hat{u}$ equal to zero. This poses problems in the integrations, particularly when one allows for a non-zero transverse momentum of constituents inside the colliding hadrons. In such case the large p_T secondary particle may originate from hard scattering process with small $\hat{t}$. In order to remove the singularity, the variables $\hat{s}$, $\hat{t}$, and $\hat{u}$ are usually replaced[19,27] by $\hat{s} + M_o^2$, $M_o^2 - \hat{t}$ and $M_o^2 - \hat{u}$ respectively, with $M_o^2 = 1.0$ GeV^2. This arbitrary cut-off procedure affects the calculations for the low transverse momentum secondaries; the effects are, however, negligible for $p_T > 3$ GeV/c.

4. The quark and gluon distribution functions. In the QCD approach, the quark distributions used for the description of large p_T processes are the same as those measured in deep inelastic lepton scattering (DIS). The relevant range of Q^2 is, however, not covered by the existing DIS data. Therefore, the effective quark distributions are extracted from

the data at some fixed value of Q^2, e.g., $Q^2 = 4$ GeV^2, and then extrapolated to high Q^2 values using the QCD evolution equations.[28] The analysis of ep or μp data is relatively insensitive to the gluon distribution inside the proton. The gluon distribution function is assumed[19] to be of the form $G_{g/p}(x,Q^2 = 4 \text{ GeV}^2) = (1 + 9x)(1 - x)^4$. The total momentum carried by the gluons, represented by the integral of $G_{g/p}$, is equal to 50% of the proton momentum.

5. Fragmentation functions. Here again the fragmentation functions are expected to be the same as measured in the e^+e^- annihilation into hadrons and to follow[29] the pattern of scaling violation similar to that of distribution functions. The e^+e^- data are not yet sufficient for their good determination. Feynman, Field and Fox[19] assumed the shapes of the quark fragmentation functions, at the reference value of $Q^2 = 4$ GeV^2, as given by their analysis of the data.[30] An example of the Q^2 dependence of $F_{u/\pi}$ is illustrated in Fig. 5 together with the gluon fragmentation function (assumed to be $F_{g/h} \sim (1 - z)^2/z$). The resulting single particle spectrum, calculated using the above-listed ingredients, does not scale. It can still be parametrised by the formula (2) but the effective power n depends now on the range of the transverse momentum and x_T. The changes of the parameter n introduced by the scale violating effects of each component of the calculation are illustrated[19] in Table 2 for the reaction $pp \to \pi^0 X$ in the range $2 \leq p_T \leq 10$ GeV/c and $x_T = 0.2$.

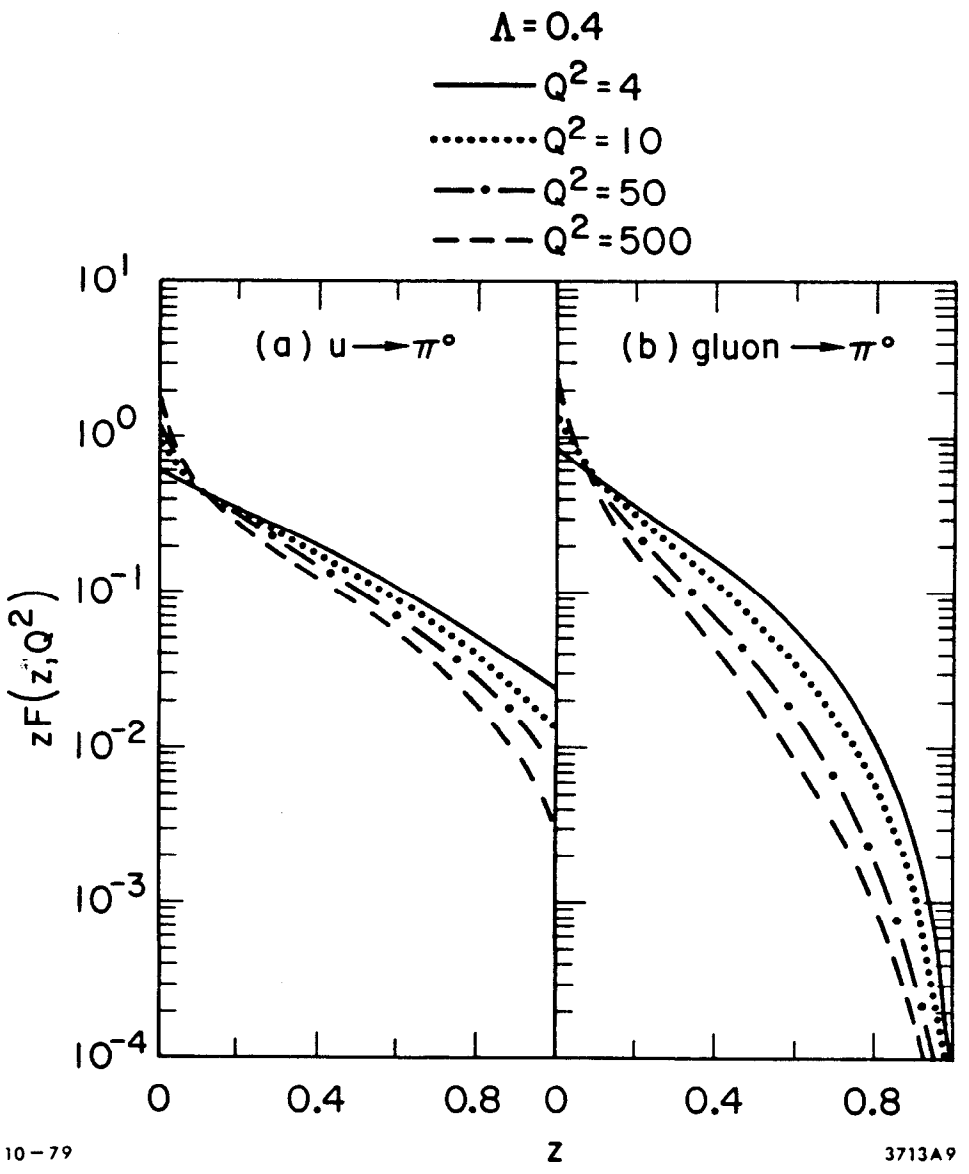

Fig. 5. Scale breaking behaviour of the fragmentation functions used by Feynman, Field and Fox[19] for the up quark and gluon.

TABLE 2

	n_{eff}
No scale breaking	4.0
$\alpha_s(Q^2)$	4.8
$G(x,Q^2)$	5.0
$F(z,Q^2)$	5.8

So far, there is an agreement among the theorists[31,32] as to the correctness of this procedure of how to introduce scale violations although there are arguments about the details. There is still a substantial freedom in parametrisation of the distribution and fragmentation functions in particular those concerning gluons. The overall philosophy seems, however, to be generally accepted. The terms discussed so far are expected to dominate the hard scattering processes at very large transverse momentum. The value of n = 5.8 is still, however, in clear disagreement with experimentally observed n ≈ 8. It is obvious, therefore, that in the framework of perturbative QCD the first order diagrams alone are not sufficient to explain the shape of the measured single particle p_T distributions and that the higher order terms are needed.

3.3 Higher Order Effects

There are in the literature two main approaches to the problem of estimating higher order corrections to large p_T processes.

1. Higher Twists or "Norther California School." Jones, Gunion and Brodsky and their collaborators[22,23] advocate that the dominant contribution in the p_T range below $p_T \sim 10$ GeV/c comes from the CIM type of diagrams, which in the QCD language are called higher twists. The subprocess cross sections for those diagrams

$$\frac{d\hat{\sigma}}{d\hat{t}} = \pi\alpha_M^2 \frac{1}{\hat{s}\hat{u}^3}$$

yield the p_T^{-8} dependence of the single particle distributions. The results have characteristic features similar to those of the Constituent Interchange Model but the calculations are now performed in the QCD framework. The phenomenological analysis of the large p_T data performed by Jones and Gunion[22] does not, however, take into account the Q^2 dependence of the first order QCD diagrams. This may lead to the overestimation of the size of the higher twist contribution because the precise normalisation of the CIM terms is uncertain.

2. Transverse Momentum Smearing or "Southern California School." Feynman, Field and Fox argue that all the higher order terms may be approximated by the assumption that partons inside colliding hadrons have non-zero momentum k_T. This transverse momentum has two components:

i) The primordial k_T due to the confinement of partons inside the hadrons. It is intrinsic to the basic parton wave function and is related through the uncertainty principle to the radius of the confining particle.

ii) The effective k_T due to the wide angle gluon bremsstrahlung. In the perturbative QCD approach it corresponds to the $2 \to 3$ particle subprocess.

Both components, illustrated in Fig. 6, occur simultaneously and in the practical calculations are described by the single gaussian function with rather large $\langle k_T \rangle$. The same arguments apply also to the

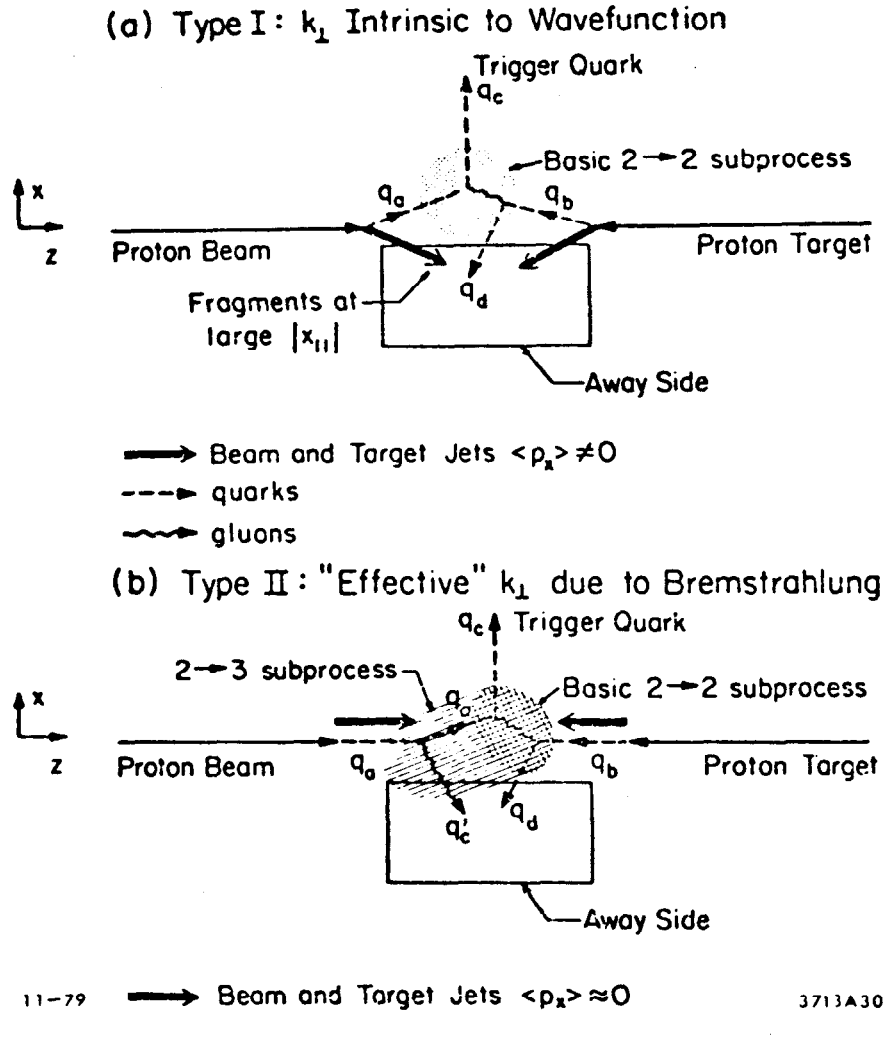

Fig. 6. Illustration of the two components of k_T smearing.

fragmentation of partons into hadrons. The values of the parameters, suggested by the dimuon data, are:

$$\text{in the distribution functions:} \quad \langle k_T \rangle_{h \to q} = 848 \text{ MeV/c} \quad ;$$

$$\text{in the fragmentation functions:} \quad \langle k_T \rangle_{q \to h} = 439 \text{ MeV/c} \quad .$$

The introduction of large k_T smearing is somewhat controversial as the results become very sensitive to the cut-off parameters. It has also been pointed out[33] that the use of the off-shell kinematics greatly reduces the effects of k_T smearing. Therefore, one should interpret the large values of intrinsic $\langle k_T \rangle$ not as a measure of the real transverse momentum of partons but as a phenomenological modeling of the neglected higher order terms such as $2 \to 3$ subprocesses, higher twist terms, etc. In such an interpretation the values of the $\langle k_T \rangle$ parameters depend on the method of calculations.

Each of the above approaches is relatively successful (with some exceptions, as discussed in the next section) in describing existing data. The indications are, that they are complementary and that the elements of both are needed. The question of the relative sizes of the effects will be answered when higher order terms in α_s contributing to the large p_T process and the radiative corrections[34] are calculated. Such corrections are important in the QCD phenomenology of the massive lepton pair production and presumably are also important here.

4. SINGLE PARTICLE DISTRIBUTIONS

In most experiments the transverse momentum spectrum is measured for the particles emitted near 90^o in the c.m. system. The signal is

expected to be clearest there and least affected by the kinematical effects near the phase space boundary. There are also existing some measurements of the p_T spectra at lower c.m. angles, the angular dependence of the distributions is not, as yet, well known.

4.1 Pions and Kaons

Until last year the available data were limited to the p_T range below $p_T \sim 8$ GeV/c and $x_T < 0.7$. The results showed very good scaling[35] within the systematic uncertainties of the experiments. They were successfully described by the parametrisation

$$E \frac{d^3\sigma}{dp^3} = A\, p_T^{-n} (1 - x_T)^m. \qquad (6)$$

The values of the parameters n and m varied[36,37] between $n \sim 8 \div 9$, $m \sim 9 \div 10$ for the charged mesons. These values were in agreement with the predictions of the dimensional counting rules. The exceptions were quoted recently[38,39] for the scaling function of the π^o production with somewhat flatter x_T distribution, $m \sim 5$. Presumably, they result from fitting the data at rather small x_T values and do not present problems for the dimensional counting rules, which apply for x_T near 1.

Last year the first ISR measurements became available[38,40,41] extending the range of the π^o spectra to $p_T \simeq 16$ GeV/c. The results presented in Fig. 7 show substantial deviations of the invariant cross section from the trend observed at lower p_T values.

The three sets of data differ by about a factor of 2 in the large p_T region; nevertheless, all three present similar trends. The departure from the p_T^{-8} behaviour is best illustrated in Fig. 8 by the

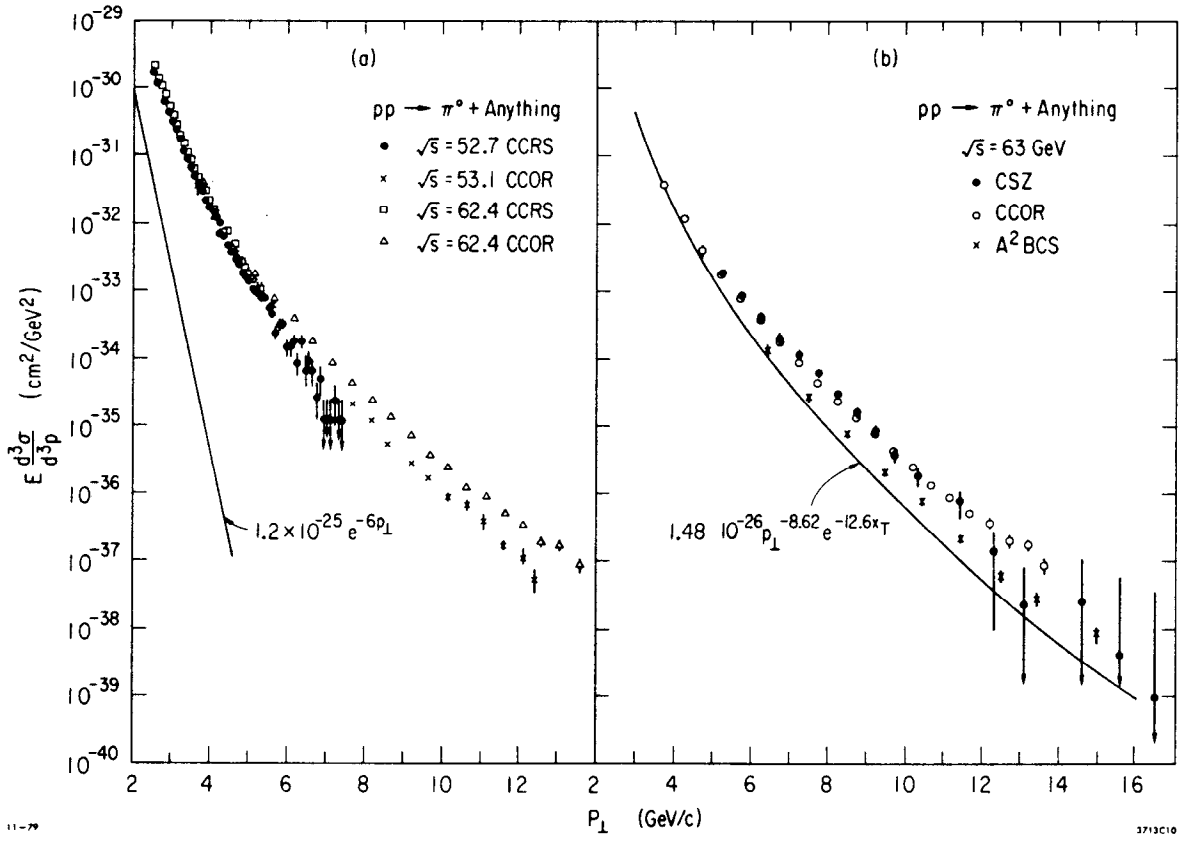

Fig. 7. Transverse momentum distribution of π^0's produced in pp collisions. The lines drawn are the extrapolations of a) fit to the low p_T data (p_T < 1 GeV/c) and b) fit to the intermediate p_T data (1 < p_T < 5 GeV/c).

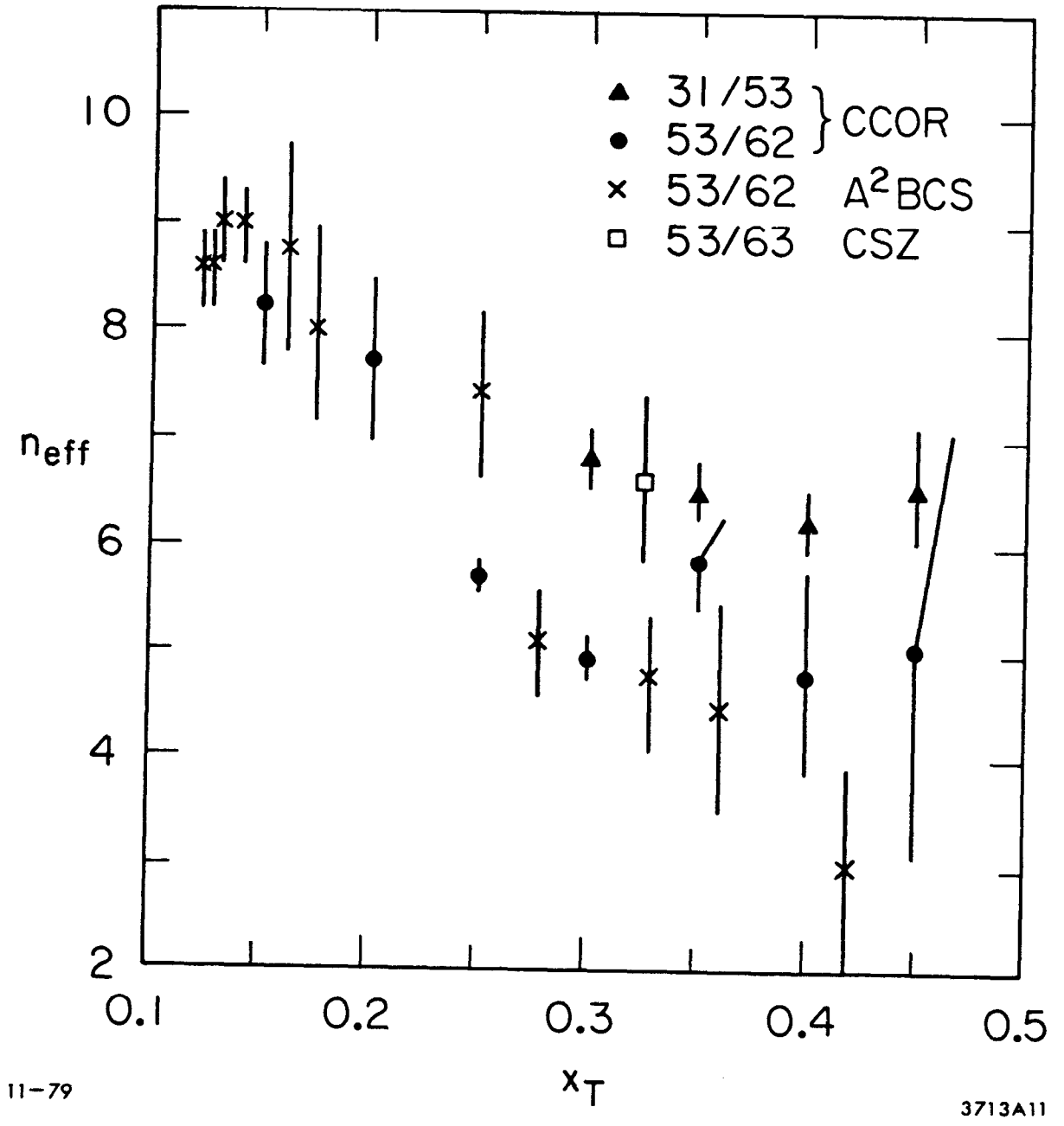

Fig. 8. Effective power n_{eff} dependence on x_T for the π^o production at the ISR.

compilation of values of the effective power n_{eff} obtained in these experiments at different values of x_T. The n_{eff} shows a systematic decrease from $n_{eff} \sim 8.5$ at $x_T = 0.1$ to $n_{eff} \sim 4 \div 6$ for $x_T > 0.3$. This behaviour is, of course, expected in QCD. It reflects the diminishing, with increasing p_T, contribution of higher order effects (k_T smearing or higher twist terms) and the emerging dominance of the first order diagrams. The examples of phenomenological description of the pion spectrum by the two approaches discussed in Section 3.3 are shown in Figs. 9 and 10.

4.2 Protons and Antiprotons

The data available until now are limited[36,37] to $p_T \lesssim 7$ GeV/c. For antiprotons they are well fitted by the formula (6) with $n \sim 9$ and $m \sim 14$. For protons, the British-Scandinavian Collaboration at the ISR obtained the value of $n = 10.38 \pm 0.34$ which is substantially smaller than $n \simeq 11.8$ measured by the Chicago-Princeton group at Fermilab. Both experiments reported similar values of $m \simeq 7.3$. The new round of experiments under way now, hopefully will resolve this discrepancy. The steep fall-off of the baryon spectrum is again compatible with the expectations of the CIM or higher twists approach, but creates problems for the proponents of the k_T smearing. Feynman and Field speculate that at these relatively small p_T values, the baryon production may be still dominated by other than hard scattering processes and that the extension of measurements to larger transverse momentum is needed for testing the QCD phenomenology. The results have, however, a much more natural explanation in terms of the CIM approach.

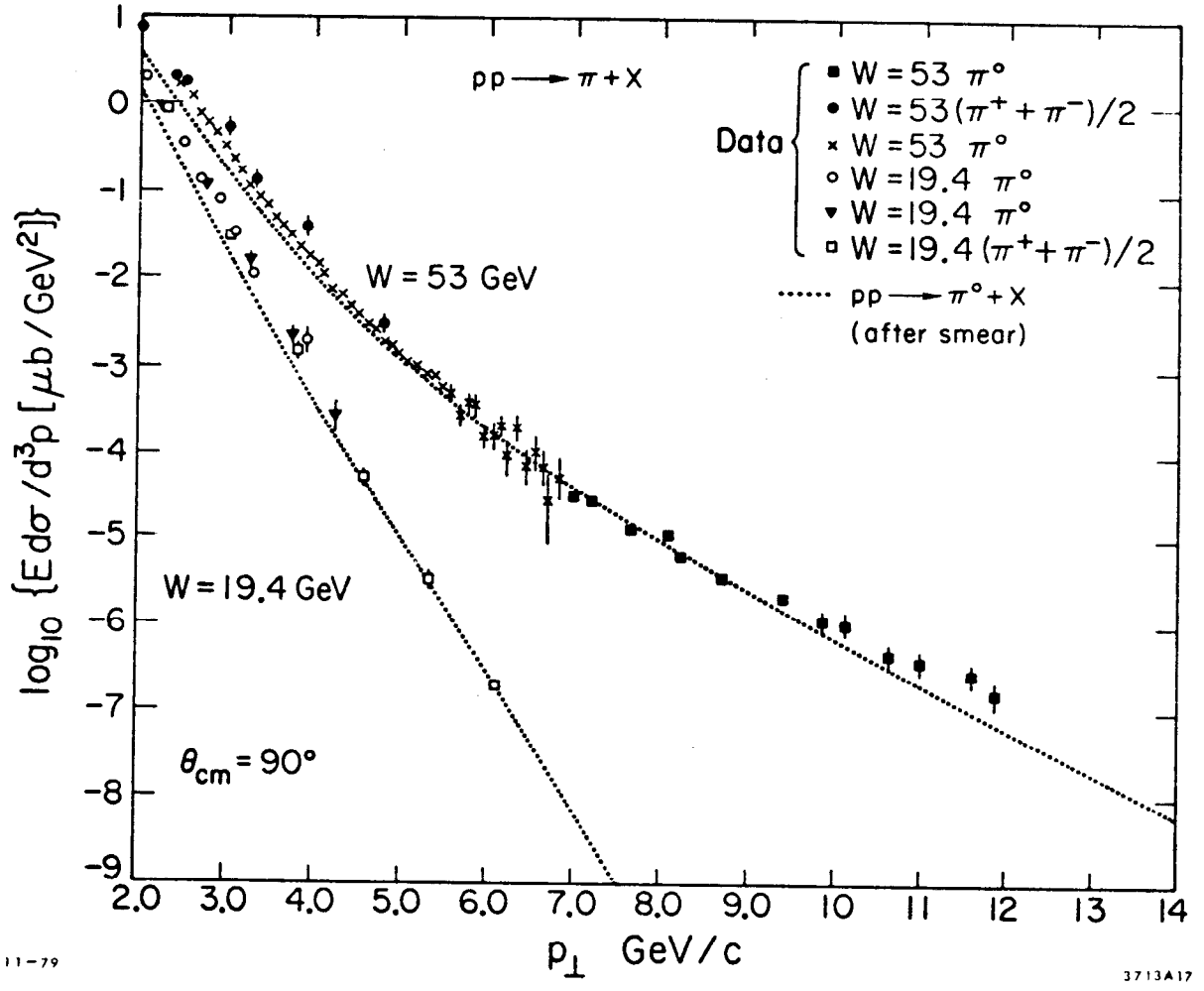

Fig. 9. Comparison of calculations of ref. 19 with the pion p_T distributions.

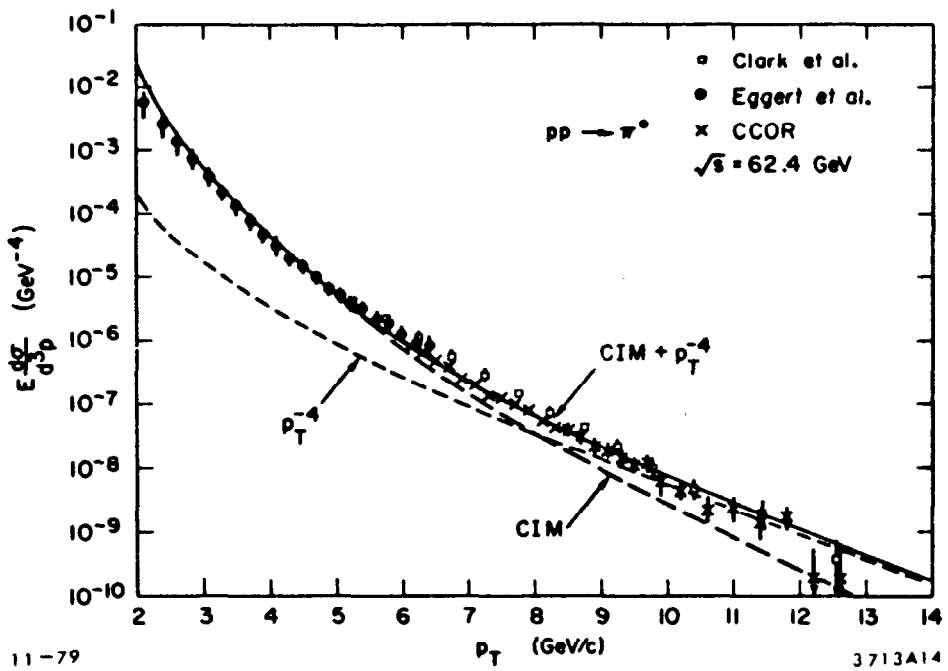

Fig. 10. Comparison of calculations of ref. 22 with the π^{o} p_T distribution.

4.3 Eta

Several experiments measured[42-44] the inclusive spectrum of η at large p_T as a by-product of the study of π^o distributions. The data show that the η spectrum is parallel, within statistics, to that of the π^o. The ratio of η/π^o production as function of transverse momentum is shown in Fig. 11. It is compatible with the value of about η/π^o = 0.5 in the range $2 \leq p_T \leq 11$ GeV/c.

4.4 Particle Ratios

Even though in pp collisions the powers n of the transverse momentum dependence of outgoing π^+ and π^- mesons are, within errors, the same, their relative yield varies with p_T. This is due to the different shapes of the $f(x_T,\theta^*)$ functions. In the QCD calculations of the first order diagrams, these functions depend on the quark and gluon distributions. In the CIM approach, they are related to the initial meson distributions inside colliding hadrons. Both phenomenological approaches, discussed in Section 3.3, encountered some difficulties in describing the data. In pp collisions the steep p_T distributions of produced baryons is reflected also in the corresponding particle ratios. The k_T smearing model of higher order terms did not reproduce successfully published results. In contrast, the data were in agreement with the CIM expectations. On the other hand, the Chicago-Princeton group measured[45] recently the ratio of π^+/π^- for the incoming π^- beam. The data, shown in Fig. 12, are almost an order of magnitude below the CIM predictions.[22] This disagreement indicates a substantial overestimation of the higher twist contributions to the large p_T processes, at least in πp reactions.

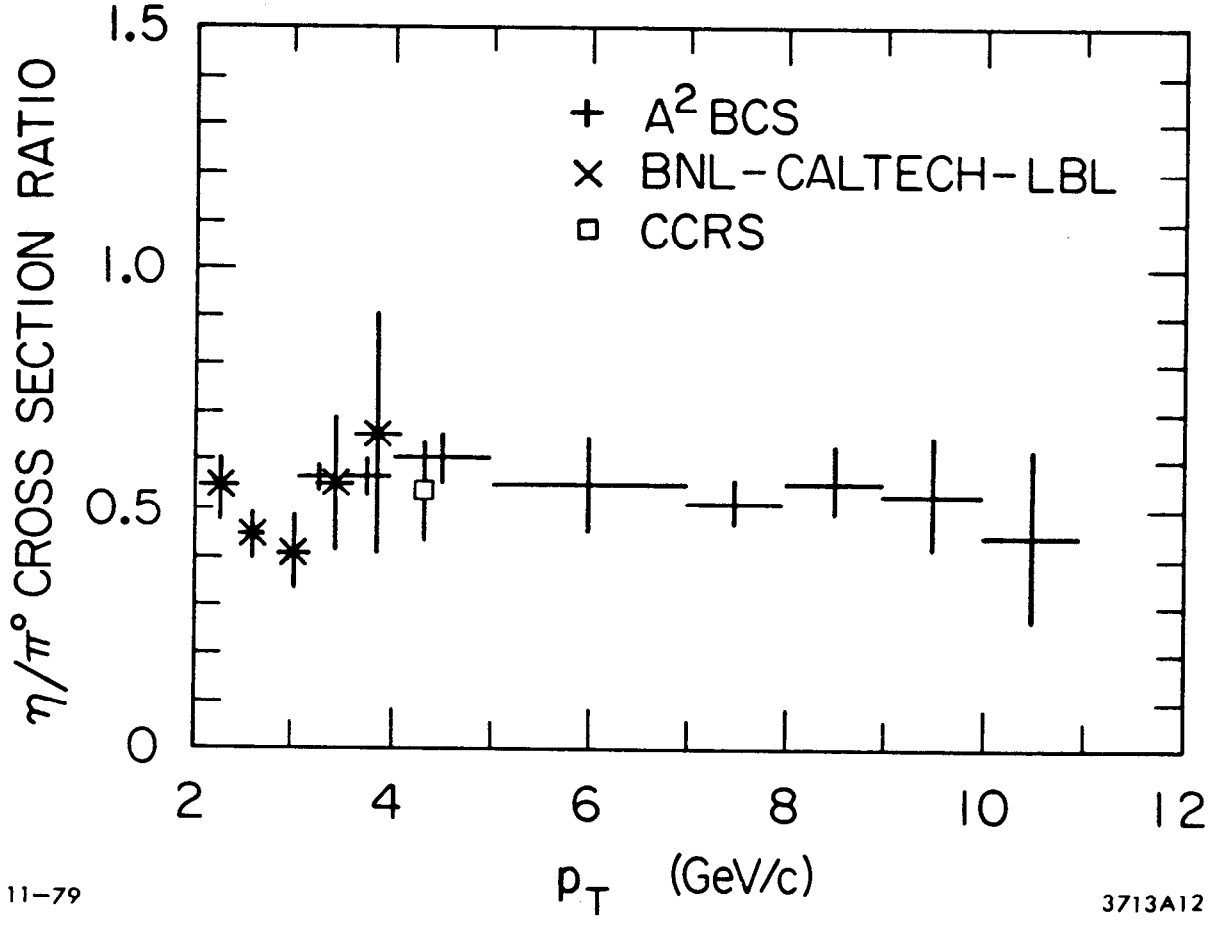

Fig. 11. The ratio of η and π^{o} cross sections as function of p_T.

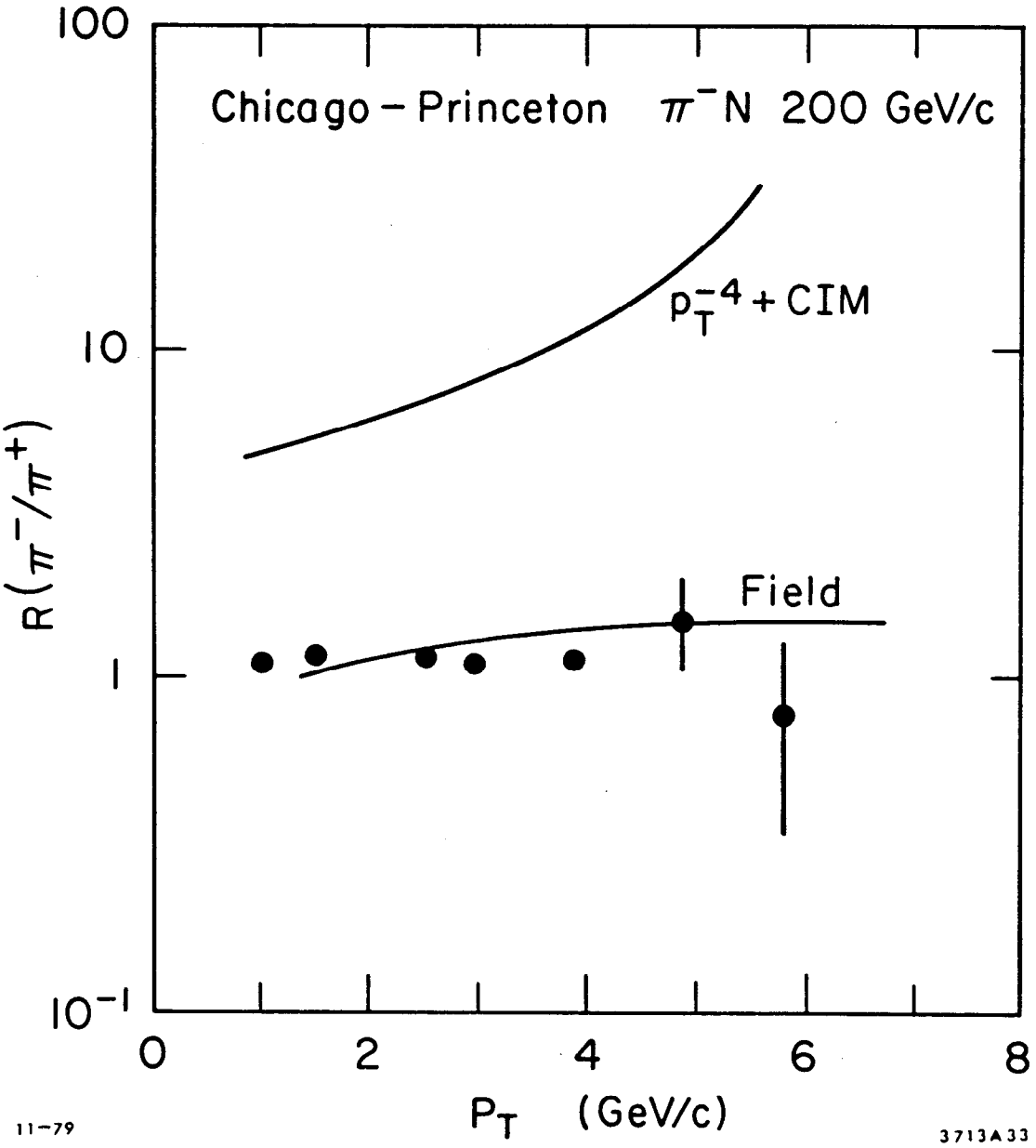

Fig. 12. The p_T dependence of the ratio of the cross sections for π^- and π^+ produced in π^-N interactions at 200 GeV/c.

4.5 Beam Ratios

In contrast to particle ratios, which depend on both distribution and fragmentation functions, the beam ratios are related mainly to the quark content of the incoming beam. In Fig. 13 are presented the data from the Caltech-UCLA-FNAL-Illinois-Indiana collaboration experiment,[46] which measured the ratios of single particle and jet production for various incoming beams. Several observations can be made here:

1. The beam ratios for single particle and jet production are similar. The scale factor of ~0.8 is compatible with value expected from the models of the fragmentation function.[19]

2. The shape of the p/π^- ratio reflects the differences of the proton and pion structure functions. At low p_T, it is approximately equal to the ratio of the pN and πN total cross sections and then falls sharply with increasing transverse momentum. This behaviour is compatible with the observations made in the studies of massive lepton pair production,[16] that the average fractional momentum of the valence quarks in the pion is larger than that of those in the proton.

3. From the observation that $R(K/\pi) \sim 1$ one may deduce that the structure function of the kaon is similar to that of the pion.

4. Finally, the ratio $R(\bar{p}/p)$, which is consistent with 1 in the p_T range below 5 GeV/c, confirms the QCD expectations that the annihilation subprocesses $q\bar{q}\rightarrow gg$ and $q\bar{q}\rightarrow M\bar{M}$ have small contributions to the large p_T processes.

4.6 Direct Photons

In the framework of Quantum Chromodynamics a real photon has a pointlike coupling to a quark. As a result, there are several possible

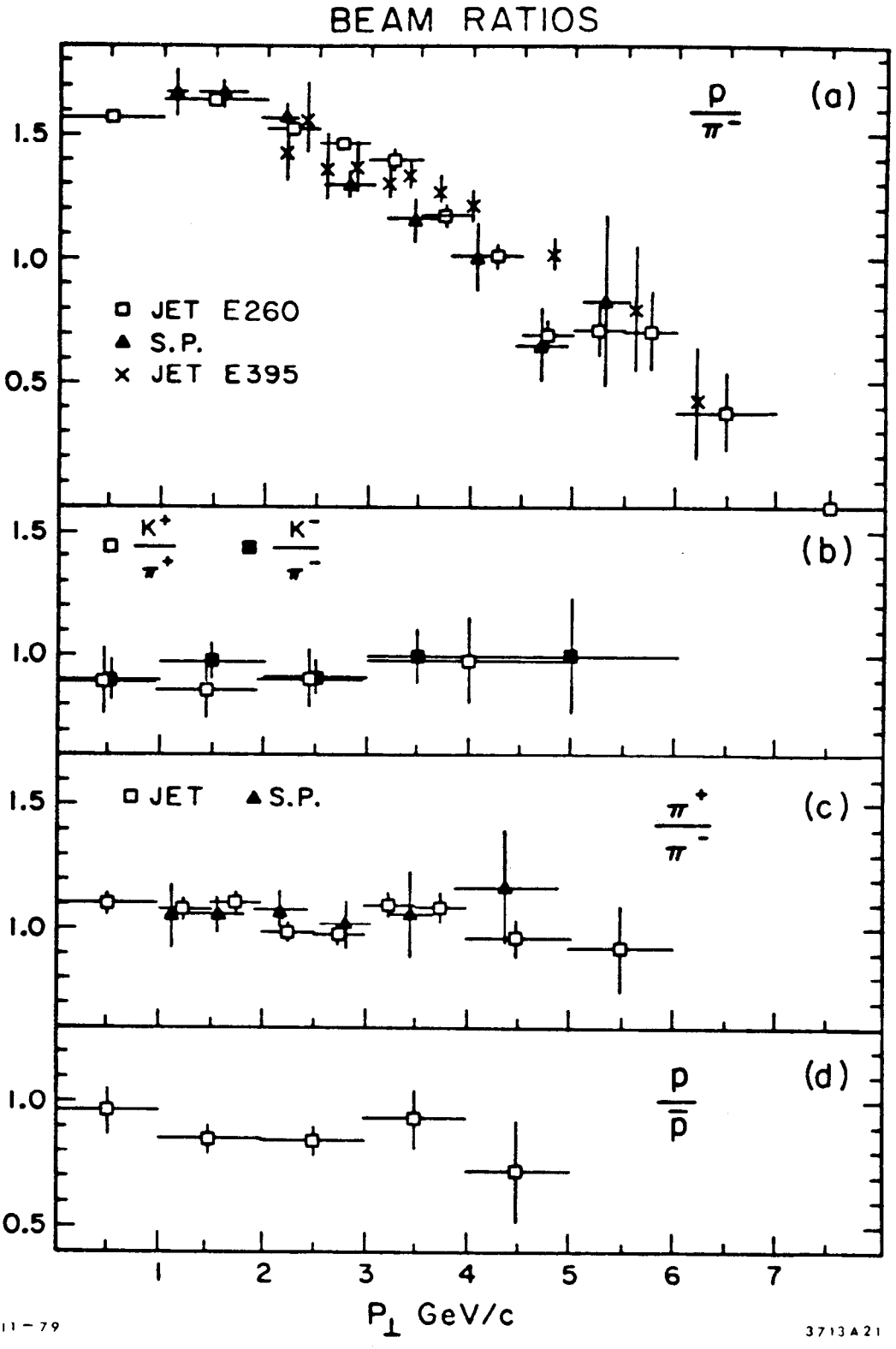

Fig. 13. Beam ratios as function of transverse momentum.

ways to produce a direct γ. In every QCD diagram with the "final state" gluon, one can replace the gluon by a photon changing simultaneously in the corresponding formulae the strong to electromagnetic coupling constant: $\alpha_s \to \alpha_{QED}$. The first order graphs are now similar to those for the Drell-Yan mechanism with largest contribution from the "Compton" scattering $qg \to q\gamma$ (see Fig. 14). The annihilation process is expected to be important in πp, Kp and $\bar{p}p$ reactions but is small in the pp collisions. In addition, direct photons may be produced[47] through the bremsstrahlung from the scattered quark or through the higher order processes of the CIM type. The CIM terms lead to the p_T^2 dependence of the γ/π ratio.

The rate of the γ production is suppressed with respect to, e.g., π^o emission, by the ratio of the coupling constants α_{QED}/α_s. On the other hand, direct photon is not subjected to the fragmentation process which introduces trigger bias discussed in Section 2.4. One may expect, therefore, the two effects to cancel resulting in the measurable γ/π^o ratio. Experimentally, however, the study of direct photon production is very difficult due to large backgrounds from π^o, η, etc., decays. Recent[48,49,80] results for the γ/π^o ratio, shown in Fig. 15, illustrate these uncertainties. The data indicate the rise of the γ/π^o ratio with increasing transverse momentum. The energy dependence of the effect remains, however, unclear mainly due to the difficulties of relative normalisation of various experimental results.

In both ABCSY and FNAL-John Hopkins experiments the γ/π^o ratio showed a trend of an increase with increasing c.m. energy. Such behaviour is consistent with the QCD expectations.

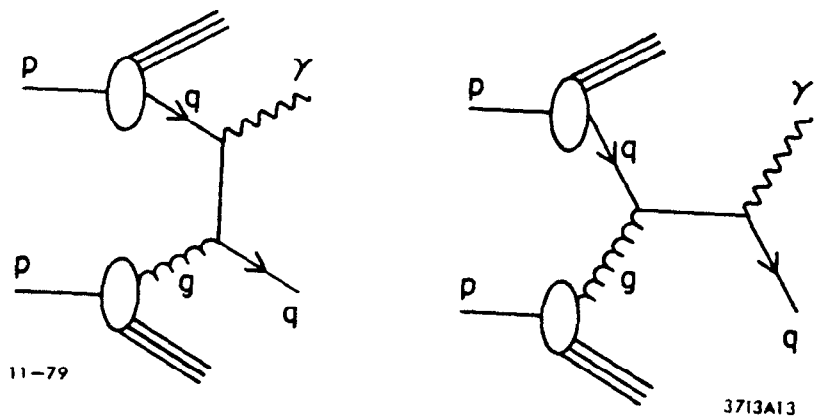

Fig. 14. First order in α_s "Compton" diagrams for direct γ production.

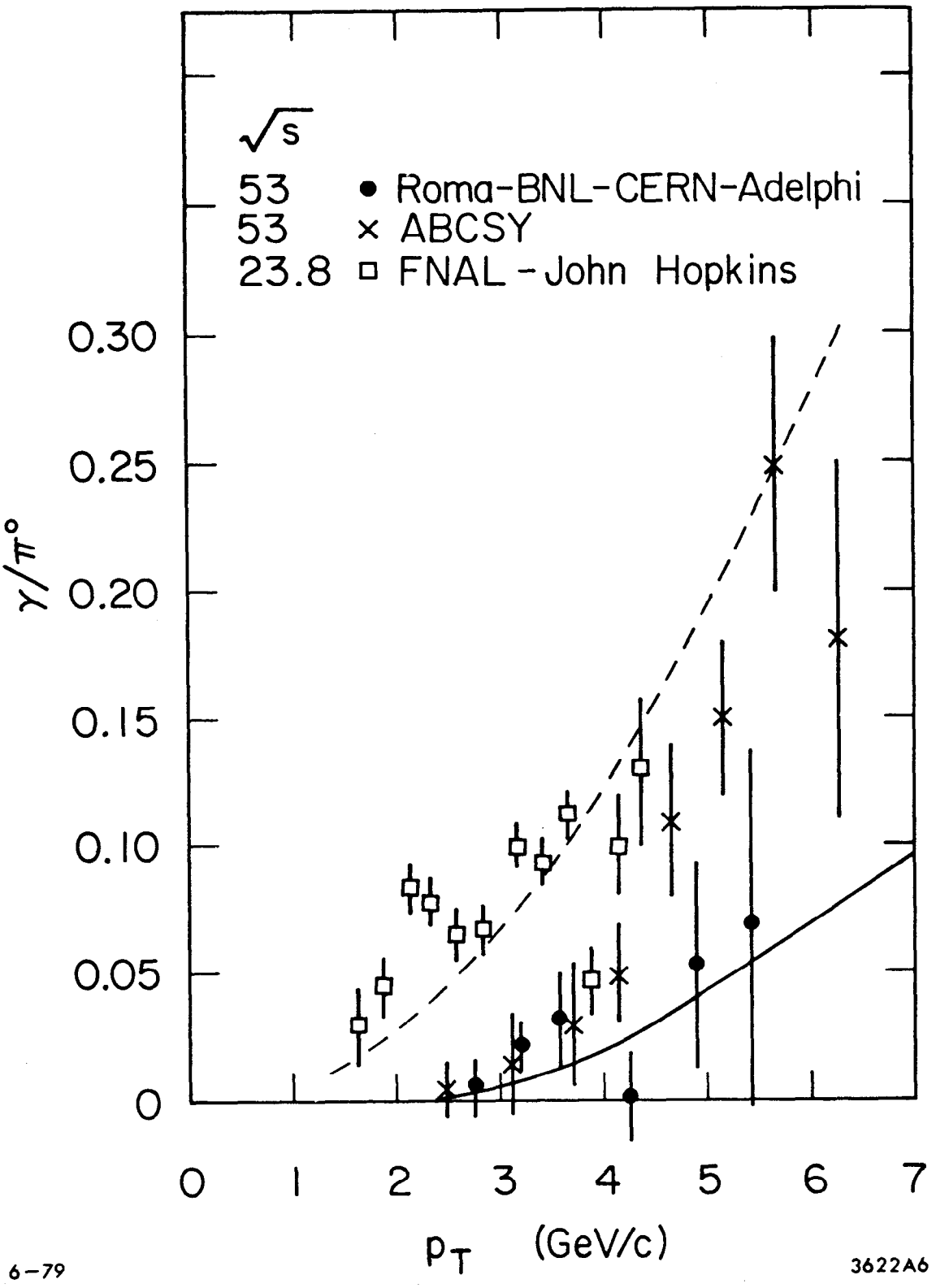

Fig. 15. The γ/π^{o} ratio as function of transverse momentum. Solid line is the result of calculations of first order QCD diagrams (ref. 26). Dashed line represents the expectations of the higher twist terms (ref. 46).

Also shown in Fig. 15 are the results of two theoretical calculations. The solid line describes the lowest order QCD calculations of Contogouris et al.[26] The dashed curve is the prediction of Rückl et al.[47] who included also the CIM terms in their calculations. The large systematic errors of the experimental measurements preclude a quantitative comparison of these curves with the data points. It is, however, evident that the direct photon signal is observed at the level expected in QCD.

5. NUCLEAR TARGET DEPENDENCE

Since the density of a heavy nuclear target is much higher than that of the hydrogen, nuclear targets are often used to study the low cross section processes. It is then an experimental problem of how to extract the cross section of a given process on single nucleon from the measurements involving heavy nuclei. It has been observed in several different experiments that the cross section has, to a good approximation, a power law behaviour as function of the nuclear number A:

$$\sigma = \sigma_o A^{\alpha}$$

In coherent processes, e.g., diffractive production, where one expects shadowing effects to exist, the value of $\alpha \approx 2/3$ is both observed experimentally and expected from the Glauber theory. On the other hand, for hard scattering processes involving partons, one does not expect any shadowing to occur. The incoming set of partons should see the target as an ensemble of point-like constituents with their numbers proportional to the number of nucleons, i.e., $\alpha = 1$. Such behaviour is indeed observed for the Drell-Yan mechanism.

The experimental measurements of the parameter α for the large p_T process are shown[36] in Fig. 16. The value of α rises with increasing transverse momentum. In contrast, however, to the lepton pair production it exceeds 1 for $p_T > 2$ GeV/c. The maximum value of α, measured so far, depends on the particle studied and is equal to 1.15, 1.3 and ~ 1.45 for the final state pions, kaons and protons respectively. As can be seen in Fig. 17, the rise with p_T is even more dramatic[50] for jets. It depends also on the beam particle and is less pronounced for the pion than for the proton beams. It should be remembered that the difference in α of ~ 0.45 translates into an order of magnitude variation of the cross section extracted from the tungsten target.

It has been suggested[51] that this phenomenon, known also as the anomalous nuclear enhancement, is due to the large transverse momentum of colliding partons. An experiment registering single particles would preferentially select such configurations in which the parton $\vec{k}_T$ points towards the trigger. The trigger bias may be thus sensitive to the variation of the parton transverse motion in different nuclei although it is not clear why it should be different for various particles. This trigger bias may be eliminated by measuring symmetric, back-to-back pairs of particles. The experimental results on symmetric dihadron production are not clear. The Columbia-FNAL-Stony Brook Group reported[52] values of α close to 1 for such triggers, while the Purdue-Michigan-FNAL Collaboration observed[53] in a somewhat different angular region that $\alpha > 1$. As the consequence of this model one may also expect that the influence of the transverse motion is smaller for the symmetric jets of particles because the fragmentation process with its k_T smearing would not affect

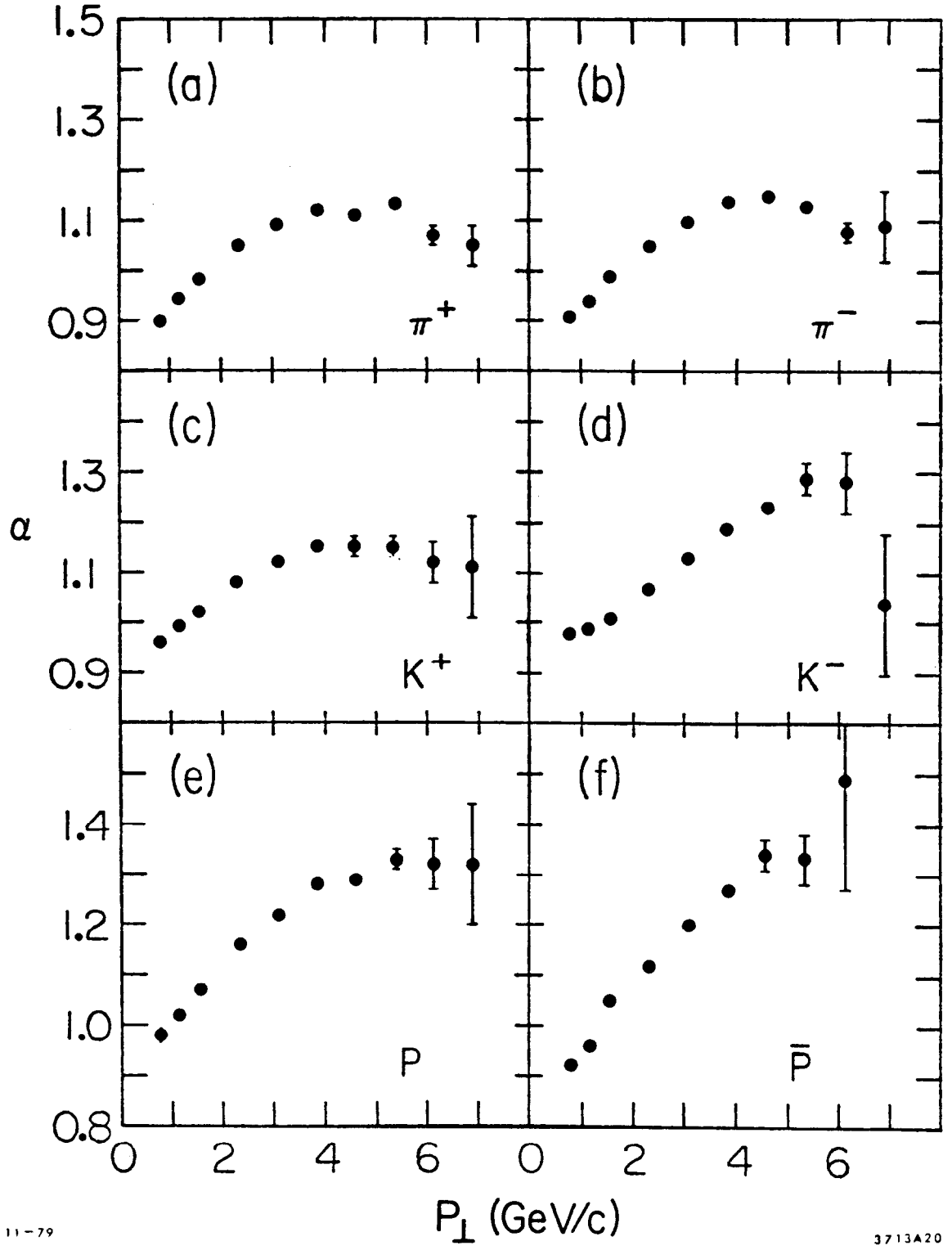

Fig. 16. The power α of the A dependence of the invariant cross sections versus p_T for the production of hadrons by 400 GeV protons.

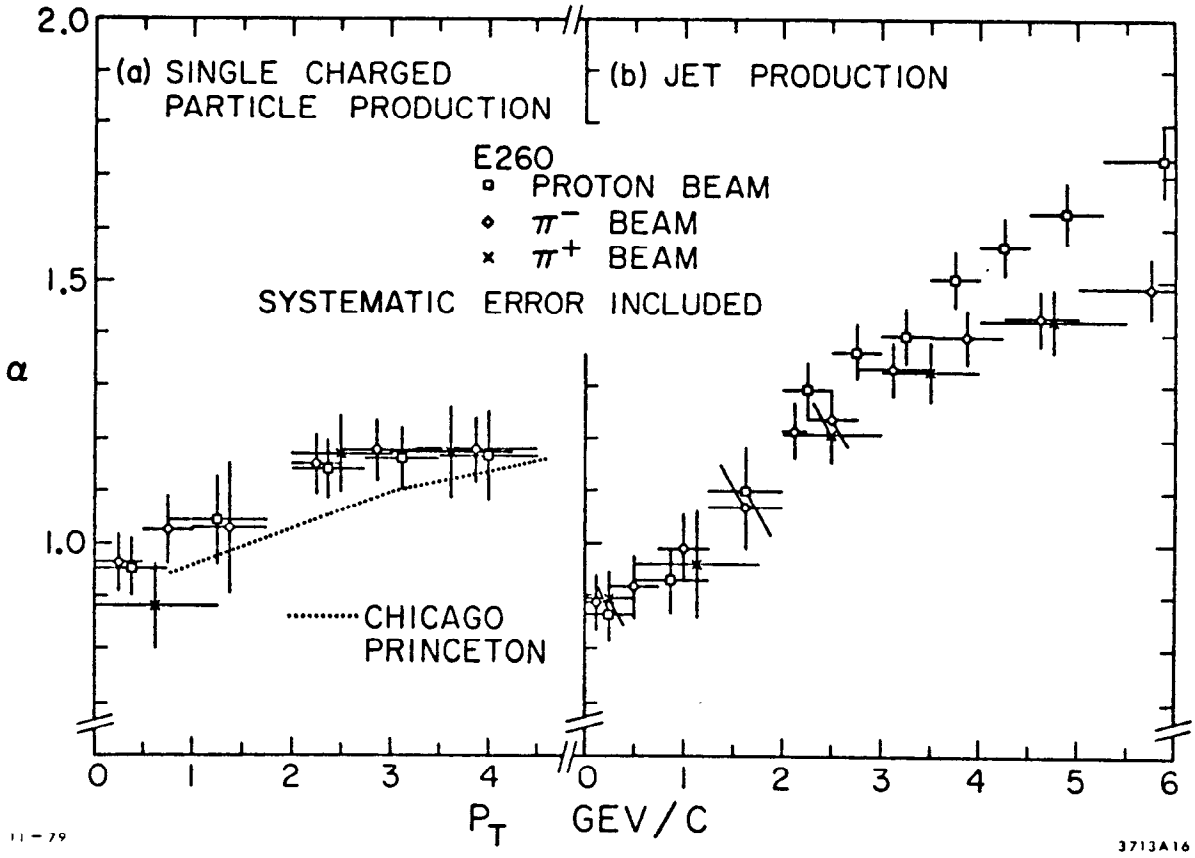

Fig. 17. The power α of the nuclear dependence versus p_T for the single particle and jet production in experiment E260 (ref. 50).

the results. The anomalous nuclear enhancement is, however, even stronger for jets than for the single particles and recent results of the experiment E-260 at Fermilab show[54] the value of $\alpha \approx 1.5$ for the symmetric pair of jets with $p_T^{jet} = 5$ GeV/c (Fig. 18).

More promising seems to be the recent proposal[55-57] that the large values of α result from multiple scattering of partons inside nuclei. The intrinsic time scale of hard processes requires the outgoing quark or gluon to fragment well outside the nucleus. Therefore, it has the opportunity for multiple interactions. Krzywicki, Engels, Petersson and Sukhatme[57] have calculated the nuclear dependence of such an effect in the framework of QCD. The general series:

$$\sigma^A/\sigma_o = A + c_1 A^{4/3} + c_2 A^{5/3} + \ldots$$

arises from final state interactions with 0, 1, 2,...nucleons in the target. Its coefficients depend on the colour factor of the partons. The effective values of α calculated from the first order QCD diagrams are listed in Table 3 for quarks and gluons.

TABLE 3

p_T(GeV/c)	5	7	9	11
α_q	1.07	1.07	1.06	1.11
α_g	1.15	1.23	1.23	1.27

As can be seen, the gluons (colour octet) interact more strongly than quarks and as a result the fraction of final state gluon jets is greatly enhanced in heavy nuclei. For example, for the uranium target and

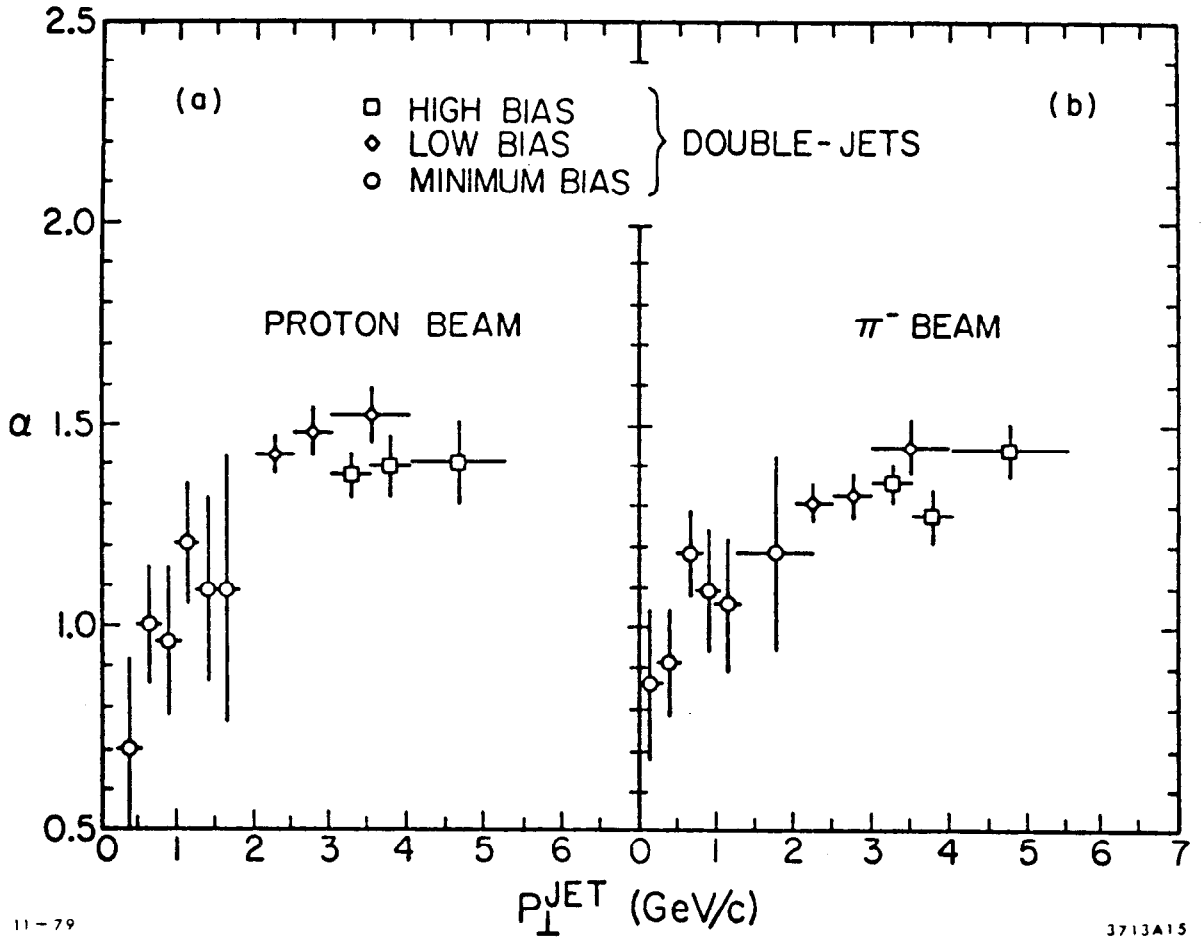

Fig. 18. The power α of the nuclear dependence versus p_T for the double jet production in experiment E260 (ref. 54).

$\alpha = 1.5$, i.e., $p_T > 7$ GeV/c, about 90% of all jets are due to the gluon fragmentation.

Of course, there may be other sources of the anomalous nuclear enhancement which contribute to the same p_T region. The calculated size of the multiple scattering effect promises, however, an opportunity to study for the first time the parton-nucleon collisions.

6. JETS

In the parton picture of large p_T processes, the scattered quark or gluon is expected to fragment[58] into several particles. The process of evolution of constituents into hadrons is not, as yet, well understood. It is usually assumed[30,58] that the outgoing quark carries a colour field in which the quark-antiquark pairs are created. The process, illustrated in Fig. 19, results in a cascade of mesons among which there may be also resonances. The final state particles are expected to have limited transverse momentum with respect to the direction of the original quark and the ensemble of all those particles is called a jet.

If one neglects the correlations induced by the colour conservation, the sum of the jet particles should represent the global features of the original quark, i.e., the sum of the momentum vectors and energies of all the final state particles should roughly correspond to the momentum and energy of the parent quark. Therefore, if one is able to identify among all hadrons in the final state those which belong to a particular jet one may study the properties of the constituents.

In the old parton model one expects four jets: two from the scattered quarks and two from the fragmentation of the spectator system.

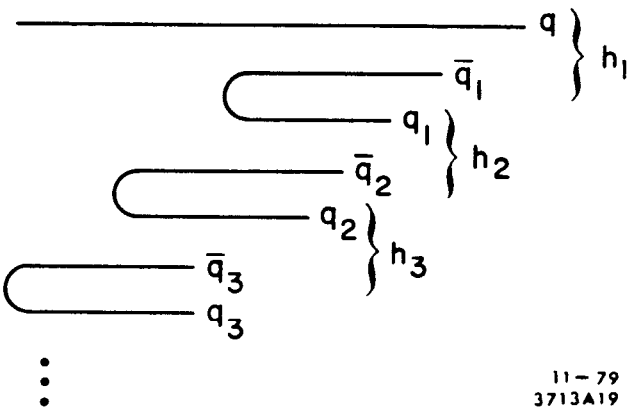

Fig. 19. Graphical illustration of the cascade fragmentation of quark into mesons.

In Quantum Chromodynamics, the situation is somewhat more complicated.[59] First, one of the scattered constituents may be identified with a gluon. The gluon fragmentation is generally assumed to proceed via the creation of the $q\bar{q}$ pair with each quark fragmenting independently. Intuitively, one expects therefore, that the jets due to the gluon fragmentation have higher multiplicity and consist of lower momentum particles than jets from the quark fragmentation. The second complication is due to the emission of gluons before or after the hard collision. The decay products of collinear gluons may coalesce with jets from the constituent decays leading to broadening of the size of the observed system. Finally, the large angle emission of gluons, i.e., the $2\rightarrow3$ elementary subprocess, is expected to lead to the additional, well separated jet in the final state. The frequency of such "five jets" events should be suppressed, however, by the power of $\alpha_s(p_T)$ with respect to that of the "four jets" events.

6.1 Trigger Bias

In order to understand the relation between the single particle and jet distributions it is important to discuss here the so-called trigger bias effect.[60,61] I will follow the example given by Ellis, Jacob and Landshoff[61] for the simple parton model. In the first approximation most of the arguments apply also to the QCD approach.

Let us assume that there is only one kind of a quark and that the fragmentation function of this quark into hadrons, $F(z)$, scales. If one ignores the transverse momentum of the fragmentation products with respect to the quark direction, the inclusive cross-section for the production of a hadron of large transverse momentum p_T at 90^o in c.m.s. is:

$$\frac{d\sigma}{dp_T} = \int_{P_T^{jet} > p_T} dP_T^{jet} \frac{d\sigma}{dP_T^{jet}} \int_0^1 dz F(z) \delta\left(p_T - zP_T^{jet}\right), \qquad (7)$$

where $d\sigma/dP_T^{jet}$ is the cross section for the production of a jet with the momentum P_T^{jet} and is usually parametrised as:

$$\frac{d\sigma}{dP_T^{jet}} = \frac{A}{(P_T^{jet})^{n-1}} .$$

The integrated form of Eq. (7) is

$$\frac{d\sigma}{dp_T} = \frac{A}{p_T^{n-1}} \int dz\, z^{n-2} F(z) \qquad (8)$$

There are two observations to be made here. First, that the p_T dependence of the single particle distribution has the same[60] power n as that of the parent jet. Second, that due to large n, the values of z close to 1 contribute most to the single particle cross section. This means that the triggering large p_T particle carries most of the jet momentum.

For the numerical estimate of the size of the trigger bias effect, it is necessary to describe the fragmentation function. The simple parametrisation[61]

$$F(z) = \frac{1}{m+1} \frac{(1-z)^m}{z}$$

yields after integration of Eq. (8):

$$\frac{d\sigma}{dp_T} = \frac{\text{const.}}{p_T^{n-1}} \left\{ \frac{m!(n-3)!}{(m+1)(m+n-2)!} \right\} .$$

For the canonical values of m and n discussed in section 4, i.e., m = 2 and n = 9, the expression in the curly bracket is equal to $^1/_{756}$.

That number represents the suppression of the single particle cross section with respect to the jet cross section due to the trigger bias.

Of course, the fragmentation function may have, in general, more complicated structure, e.g.,[7]

$$F(z) = B(1 - z)^m/z + K\delta(1 - z) + L + \ldots \quad ,$$

where the additional terms correspond to configurations in which the jet fragments into one particle only, two-body resonance, etc.

In QCD, the fragmentation function $F(z)$ is not expected to scale. Therefore, the jet cross section does not have necessarily the same shape as the single particle distribution. Nevertheless, in spite of the small deviations introduced by the scale violation and the complications arising from the summation of many terms, the global effects of the trigger bias are expected to remain unchanged.

6.2 Jet Experiments

There are at present three experiments at Fermilab which have triggered on large p_T jets. Two of them (E260 and E395) have already published some of their results, while the analysis of the third (E236) is still in progress. The details of those experiments have been recently extensively reviewed,[62,63] therefore I will comment only on their main features.

The jet experiments select events with large transverse energy $E \gtrsim E_o$ carried by the set of particles travelling together. Such triggers are obtained with the help of calorimeters. The tracking and particle identification devices situated between the target and the calorimeter provide the measurements of the number and type of particles in the jet.

The experiment E260 has in addition a magnet allowing for the measurement of the particles' momenta (see Fig. 20). Both E260 and E395 have a major drawback of being unable to avoid the trigger bias introduced by the finite size of the calorimeters. In both cases some of the jet particles may remain undetected if they are emitted outside the angular acceptance of the apparatus. On the other hand, some of the particles not belonging to the jet, e.g., originating from the spectator jets, may enter the calorimeter thus increasing the measured energy. The analysis of the data involve, therefore, rather complicated, model dependent Monte Carlo simulations. Since the raw measurements of the two experiments are corrected for different and somewhat complementary biases, it is quite encouraging to notice that the final results are similar.

In Fig. 21 is presented the comparison of the cross section[46] for the jet production measured in the experiment E260 with that of the single particle data obtained by the Chicago-Princeton group.[36] The effect of the trigger bias is clearly seen. The jet cross section is more than two orders of magnitude higher than the pion data. The absolute cross section estimates of experiment E395 agree, within factor of four, with the E260 results. Also shown in Fig. 21 are the QCD calculations[19] of the jet cross section. The two curves, which correspond to the production of jets of a given energy or transverse momentum, differ by a factor of about 15. This difference reflects the uncertainty in the QCD phenomenology whether the relevant variable is the energy or momentum of the jet particles. The sum of the masses involved is usually of the order of 1 GeV and due to the steeply falling distributions, it introduces a substantial variation in the estimates of the jet cross section.

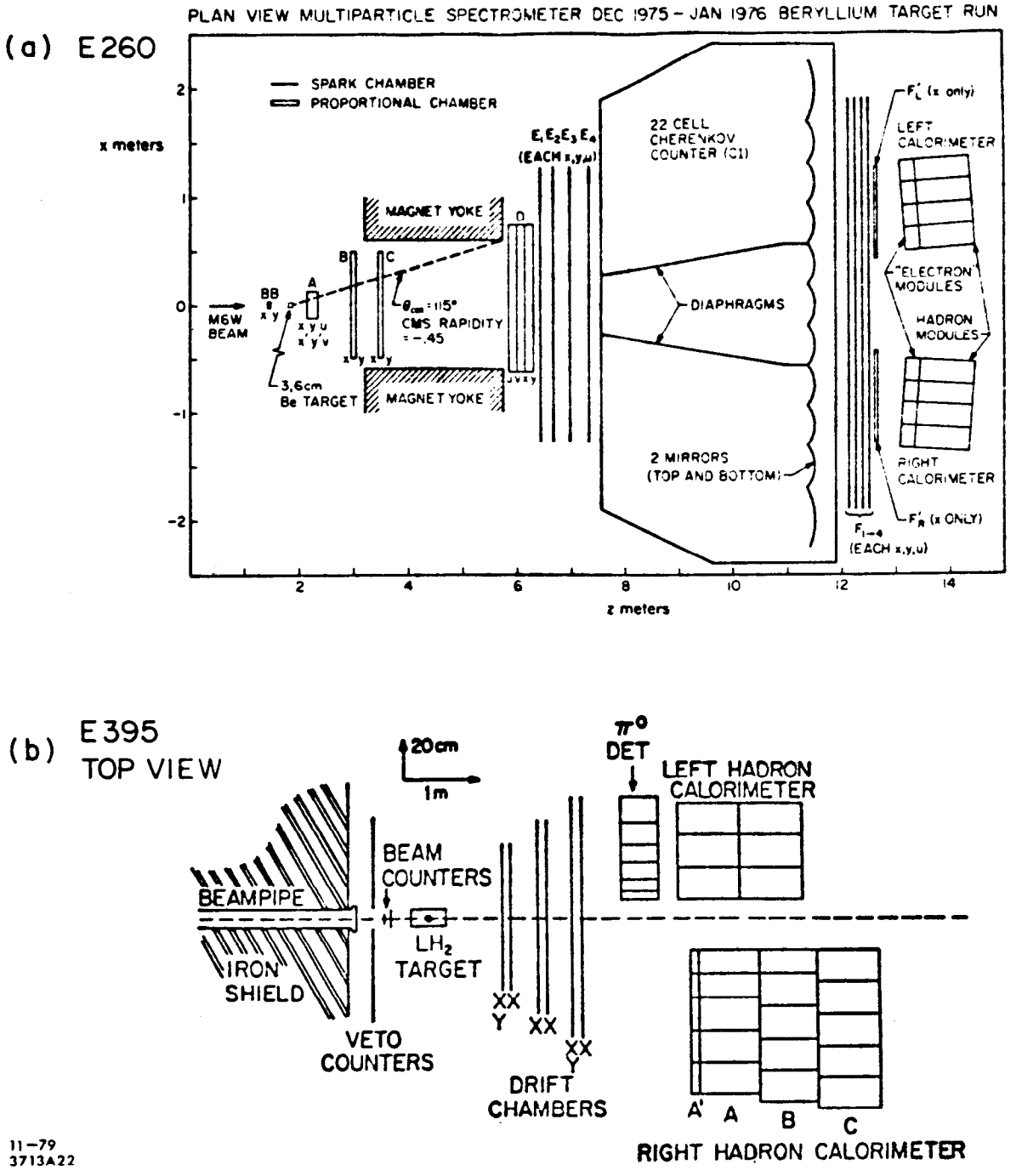

Fig. 20. The layouts of the jet experiments, a) E260, b) E395.

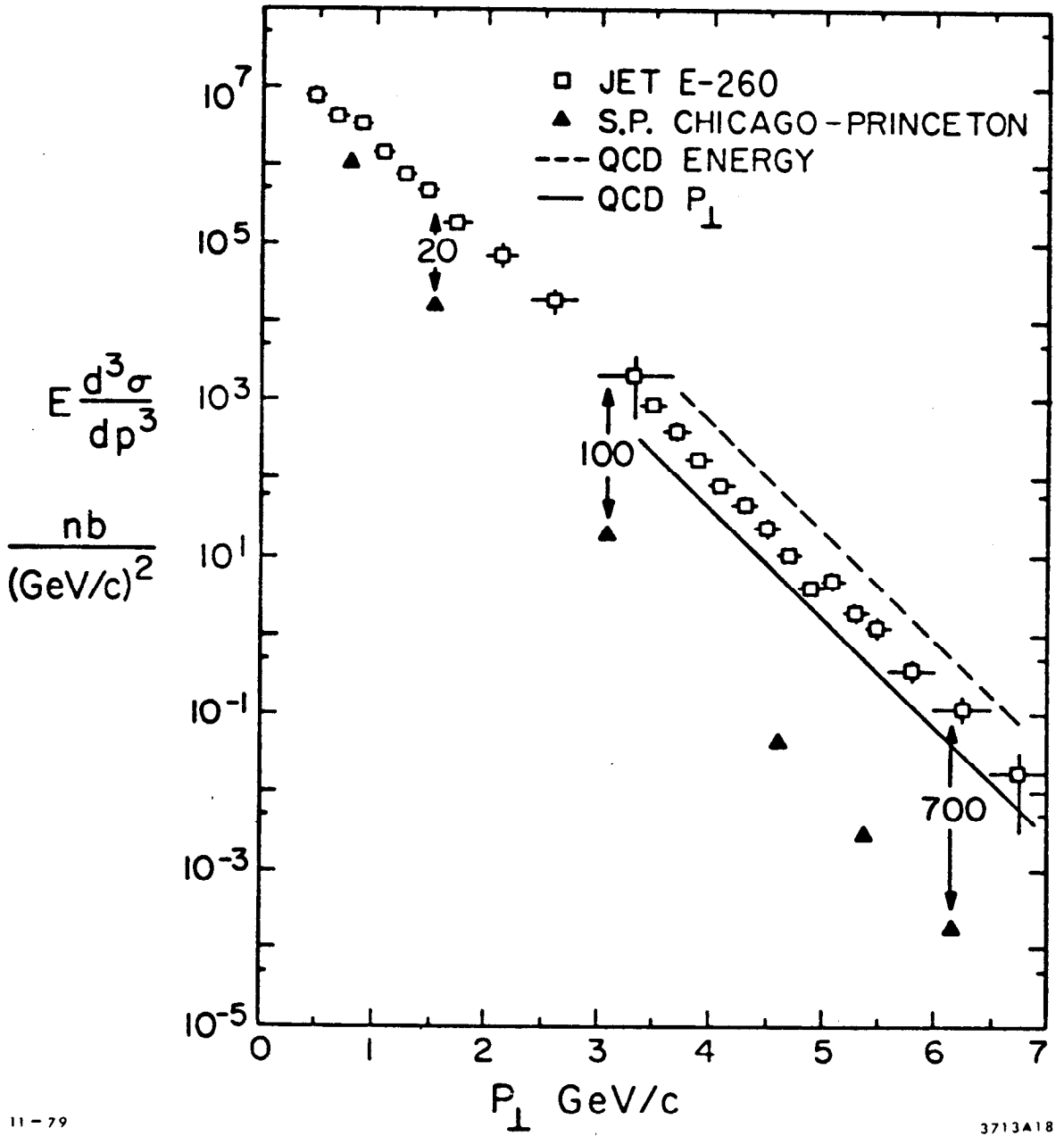

Fig. 21. Invariant cross section for pp→jet + X compared with single particle data of the Chicago-Princeton Collaboration. Also shown are the results of QCD calculations described in text.

7. JET STRUCTURE OF LARGE p_T EVENTS

In the parton model description of the large p_T processes, depicted in Fig. 1, one expects four jets. The two spectator jets should follow the directions of the beam and the target in the c.m.s. and the two jets from scattered constituents, called the "towards" and "away" jets, should balance the transverse momentum of each other. Such picture is only slightly modified in the QCD approach and the main effort of the past few years has been directed towards the identification of those four jets.[64] While the study of each individual jet provides the information about the process of fragmentation of constituents into hadrons, the tests of the description of basic interactions may be obtained only by studying the correlations among the jets.

The separation of particles belonging to a particular jet is not, however, straightforward. To illustrate the problem, in Fig. 22 is presented the density of particles associated with a large p_T trigger at 90° in the c.m.s. obtained by the British-French-Scandinavian Collaboration[65] at the ISR. This density is normalised to the same distribution obtained without requirement of the large p_T trigger (minimum bias events) in order to take into account the acceptance problems. As can be seen there is a small but distinct bump around the direction of the trigger, which corresponds to the towards jet. The broad enhancement on the opposite side represents a superposition of many away jets emitted at different c.m. angles. The strong overlap of the particles belonging to different jets, in particular those with small p_T, makes the separation of jets somewhat model dependent. Therefore, one should take the numerical results of the jet studies always with a grain of salt.

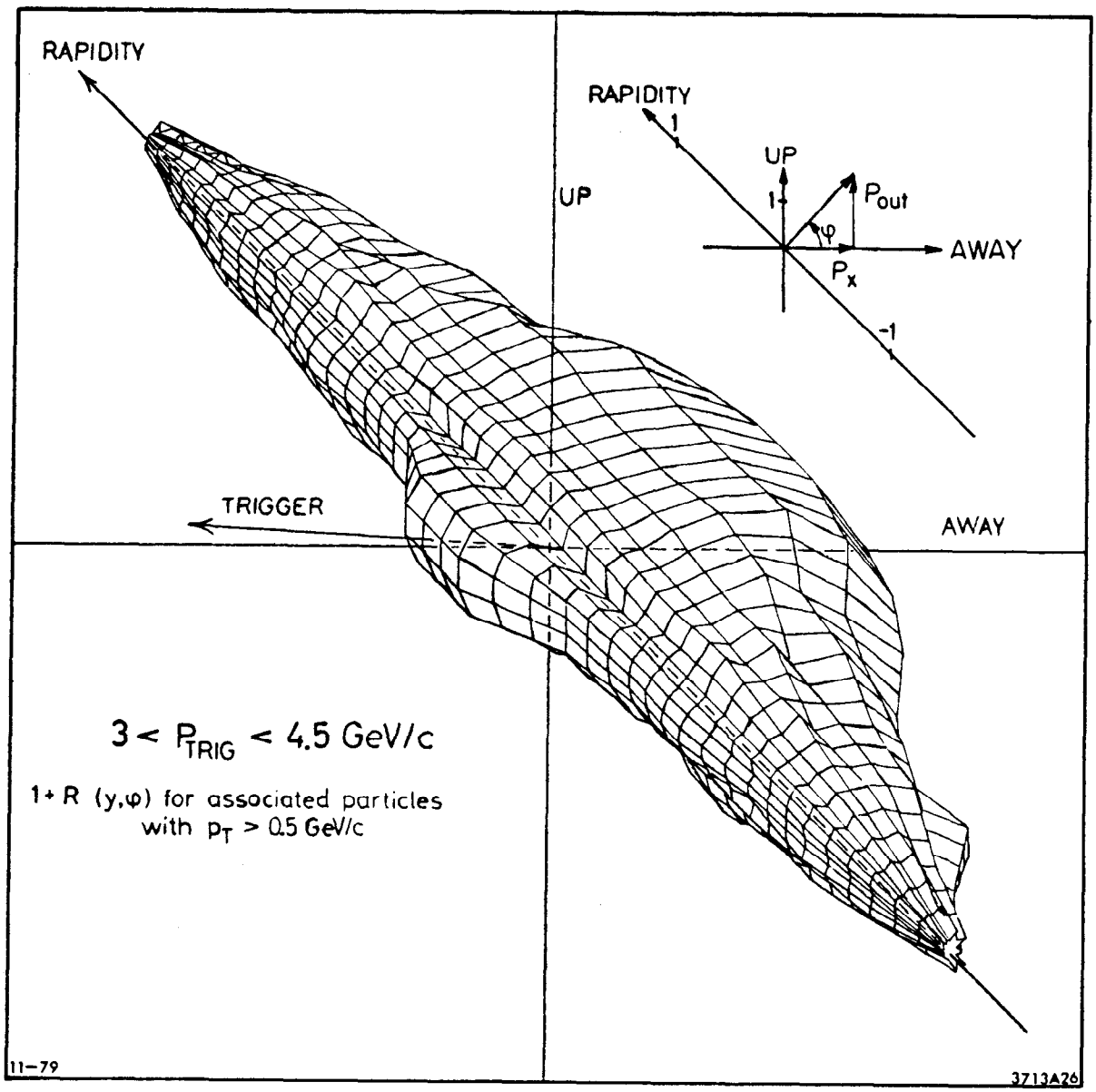

Fig. 22. The average distribution of charged particles with p_T < 500 MeV/c in large p_T events relative to the distribution observed in minimum bias events. Also shown are the definitions of variables used in jet analysis.

Also shown in Fig. 22 are the definitions of some of the variables used in the jet studies. The two azimuthal regions containing the scattered jets are usually defined as $\Delta\phi = \pm(30° \div 40°)$ around (towards) or opposite (away) to the trigger. The total momentum of the jet is defined as the sum of momenta vectors of its fragments $\vec{P}_{jet} = \sum_i \vec{p}_i$. For each individual particle in the away trigger the p_{out} and p_x describe the components of transverse momentum out of the trigger plane and balancing the momentum of the trigger jet respectively. In case when the trigger and away jets have equal momenta, the reduced component of p_x : $x_E = p_x/P_{jet}$ is equivalent to the variable z used in fragmentation function, while p_{out} describes the intrinsic parton transverse momentum.

7.1 Towards Jet

The evidence for the towards jet, although clearly seen in Fig. 22, is somewhat better documented in Figs. 23 and 24. The azimuthal distributions of charged secondaries associated with large p_T ($p_T > 7$ GeV/c) neutral pion (see Fig. 23) show[66] strong peak at the azimuth of the trigger. The effect is practically independent of the p_T and the rapidity of the trigger. Similarly, the secondaries in the same hemisphere are correlated with triggering particle in rapidity (Fig. 24). The range of these correlations allow for the estimate of the size of the towards jet as $\Delta y \sim \pm 0.75$ and $\Delta\phi \sim \pm(30° \div 45°)$. It should be remembered, however, that the jet is distorted by the trigger bias, which preferentially selects narrow configurations.

The effective mass distributions of the triggering particle and of the identified secondaries, shown in Fig. 25, display prominent peaks

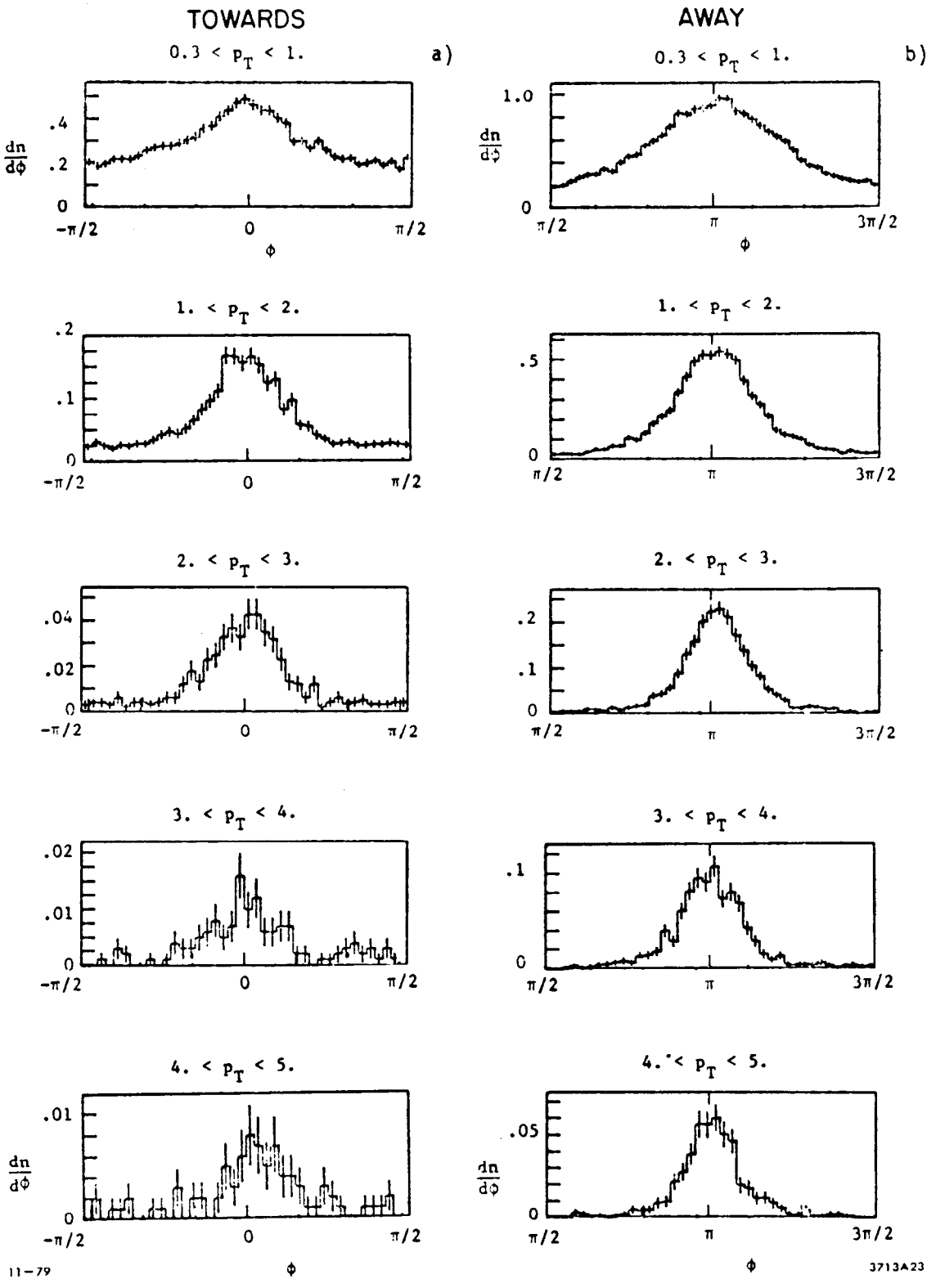

Fig. 23. Azimuthal correlation of charged particles relative to triggering π^o on a) same side and b) away side. The plots correspond to 1 GeV/c intervals in p_T of the charged particles. The transverse momentum of trigger π^o is p_T > 7 GeV/c (ref. 66).

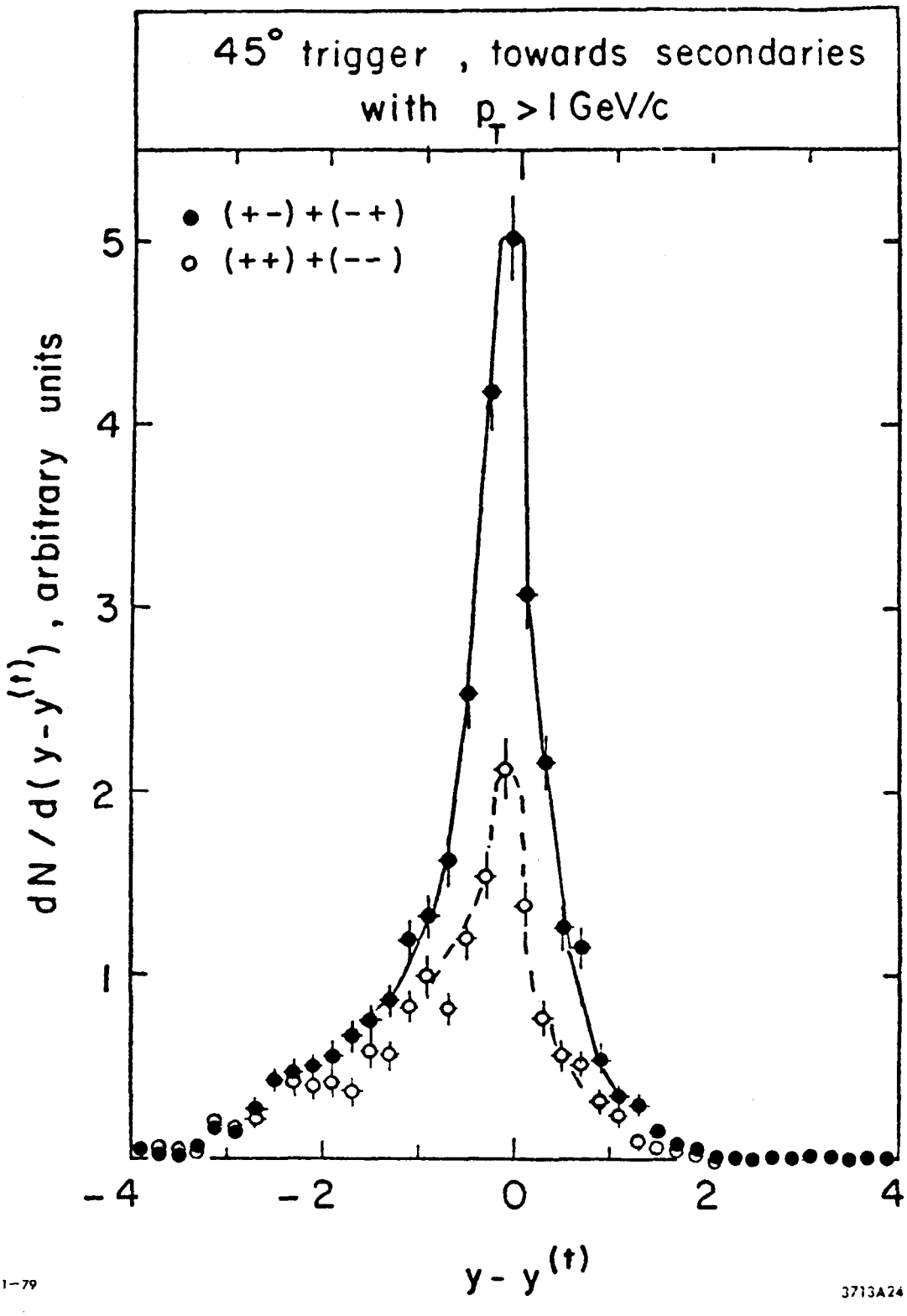

Fig. 24. Distribution of towards secondaries with $p_T > 1$ GeV/c as function of rapidity relative to the trigger rapidity, for different charge combinations of trigger and secondary (ref. 71).

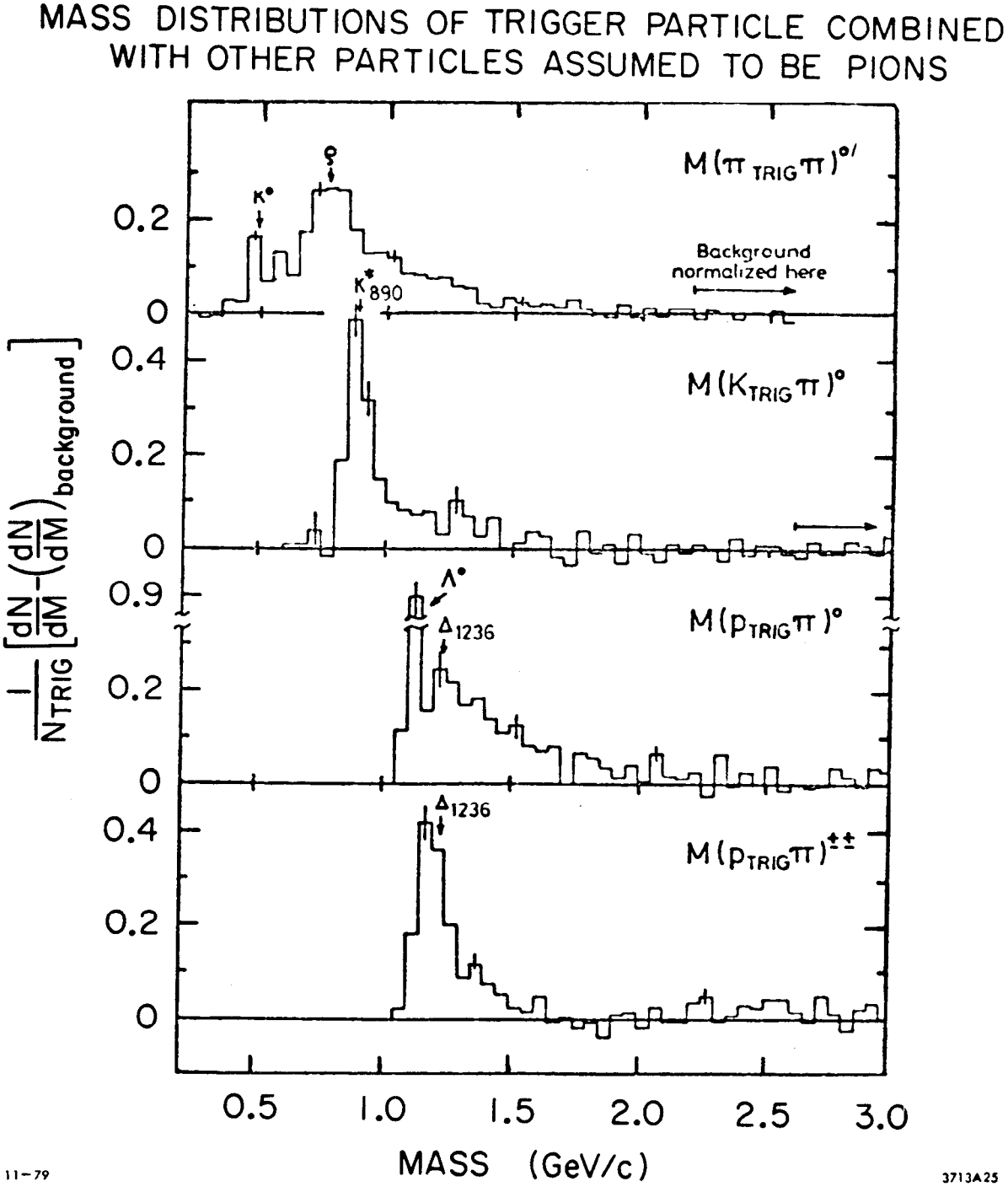

Fig. 25. The two-particle mass distributions of the systems of a trigger particle combined with other particles in the event. A background spectrum has been subtracted (ref. 65).

corresponding to ρ^0, K* (890), $\Delta^{++}(1236)$, etc. The resonances production is responsible, however, only for a small fraction of the large p_T triggers. For example, the British-French-Scandinavian Collaboration estimated[67] that only about 12% of the charged pions in the p_T range $2.2 \leq p_T \leq 3.0$ GeV/c originate from the ρ^0 decays. Nevertheless, the relative yield of resonances is comparable to that of e.g., pions at the same value of transverse momentum. This is due to the fact that the invariant distribution is a steeply falling function of p_T and even small Q values of the resonance decay lead to big corrections of the measured cross sections. The ratio of the cross sections of $\rho^0/\frac{1}{2}(\pi^+ + \pi^-)$ was found to be compatible with 1 for $p_T > 2$ GeV/c. Similarly the CERN-Saclay group measured[68] $(\rho^+ + \rho^-)/\pi^0 \approx 1$. In addition to the results mentioned above, also the observation of strong same charge correlations (see Figure 24) indicate that the production of resonances is not sufficient to explain the origin of all large p_T triggers.

Having established the existence of the towards jet we can turn now to the problem of its properties. The studies are, however, difficult because of the trigger bias and because the number of associated particles clearly distinguishable from the background is small, usually of the order of few percent per event. The methods used vary from group to group. They include in general the three following steps:

1. Selection of candidate particles by, e.g., rapidity, azimuth and p_T cuts;

2. estimate of the jet axis, e.g., as a vector sum of momenta of selected particles;

3. estimate of the background, e.g., by mixing tracks from different events.

The results depend, of course, on the details of the procedure, acceptance, cuts, etc. The answers obtained by different groups are, however, in the same ballpark. The distribution of transverse momentum of the particles with respect to the jet axis, k_T, exhibits a smooth exponential behaviour (see Fig. 26). The exponent of this distribution measures the average value of k_T. The values of $\langle k_T \rangle$ = 386 ±7 MeV/C for all neutral secondaries and $\langle k_T \rangle$ = 589 ±14 MeV/c for charged secondaries, observed by the CERN-Saclay group may be compared with $\langle k_T \rangle$ = 520 ±50 MeV/c estimated by the British-Scandinavian Collaboration.

The distribution of z, the fraction of the jet momentum carried by its each component, was observed to scale in most of the experiments. The exception was quoted by the CCOR Collaboration[69] which found the average value of <z> decreasing with p_T of the trigger.

7.2 Away Jet

The evidence for the away jet is not so clear as in the case of towards jet. As has been seen in Figs. 22 and 23b, there is an apparent azimuthal correlation in the direction opposite to that of the trigger. Such tendency of back-to-back configuration may result, however, from the transverse momentum conservation in the experiments with incomplete solid angle coverage or in which certain particle types remain undetected. In such case, illustrated in Figs. 27a and 27b, the trigger preferentially selects events with smaller missing transverse momentum p_T^{miss}. In order to correct for the possible experimental bias the A^2BCS Collaboration

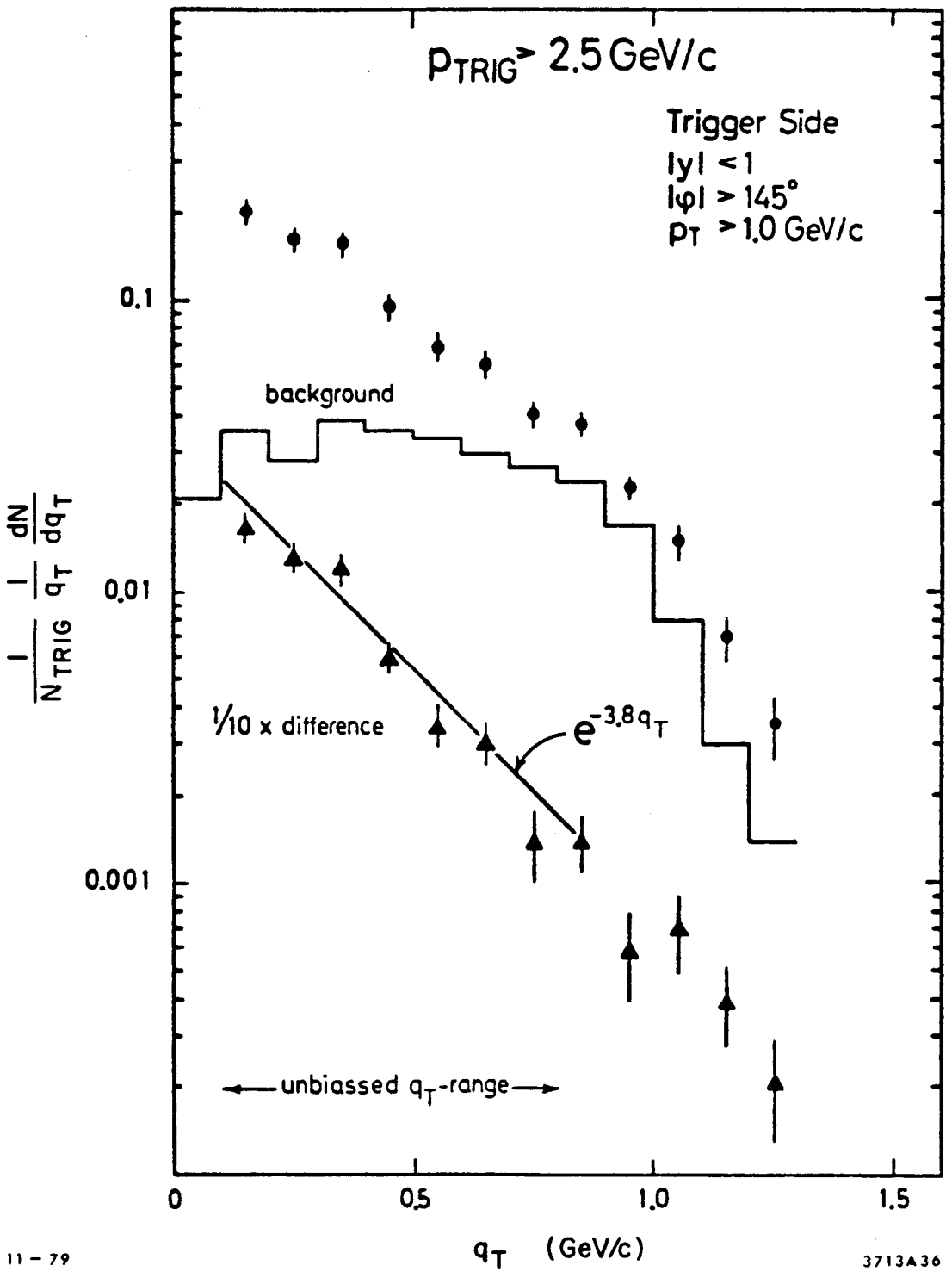

Fig. 26. The distribution $^{1}/N_{TRIG}$ ($^{1}/q_T$) dN/dq_T for the trigger side jet. The background has been estimated by taking pairs of particles from different events. The exponent translates to the average $\langle k_T \rangle$ = 520 ± 50 MeV/c.

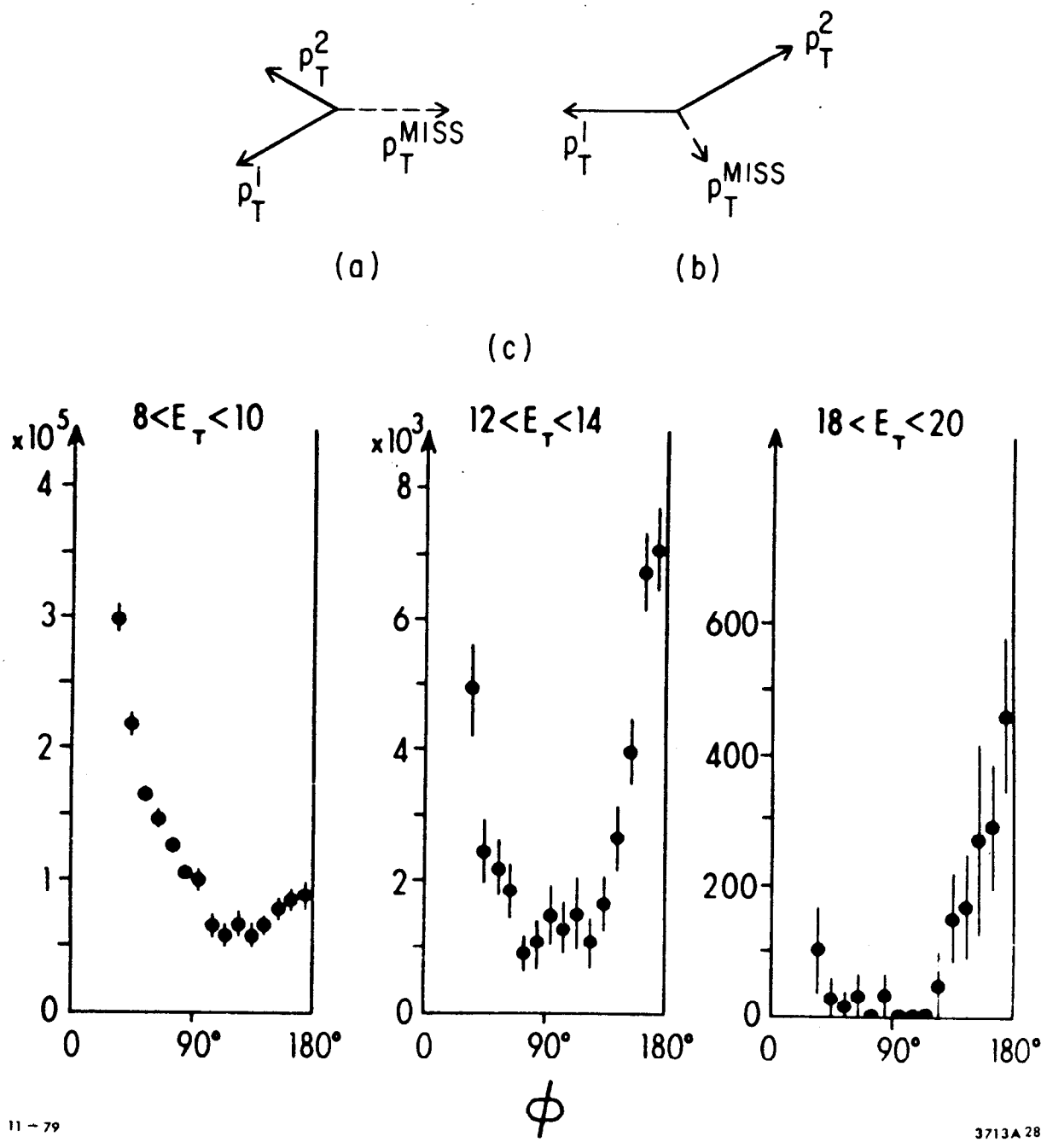

Fig. 27. The azimuthal corrleations of two large p_T π^o's for different values of $E_T = p_T^1 + p_T^2 + p_T^{miss}$ (ref. 70).

studied[70] the correlations of the large p_T π^o pairs in terms of the total energy radiated transversely $E_T = p_T^1 + p_T^2 + p_T^{miss}$. The results, shown in Fig. 27c indicate a strong coplanarity of the two π^o's at large values of their transverse momentum. Also here, the enhancement in the azimuthal distributions is limited to $\sim \pm(30° - 45°)$ around the direction opposite to the trigger.

It is, however, not easy to localise the away jet in rapidity. The density of particles opposite to the trigger (see Fig. 22) shows a broad enhancement which covers the range of ±3 units of y independently of the rapidity of the trigger. In the parton model this behaviour is explained by a Lorenz boost of the two collinear jets from their own $q\bar{q}$ rest frame to the overall c.m. system. The direction of the towards jet is fixed by the experimental trigger and the observed enhancement on the opposite side is the result of superposition of many away jets. In order to find those jets on the event to event basis, the CERN-College de France-Heidelberg-Karlsruhe Collaboration proposed[71] a procedure in which a particle with largest p_T opposite to the trigger is selected as the most likely candidate for the leading particle in the away jet. The remaining particles show then strong rapidity correlations with such "jet leader." The range of the correlations, illustrated in Fig. 28, spans about ±0.75 units of y and is similar to the width of the towards jet. It is important, however, to remember that this procedure introduces also here the trigger bias similar to that of the towards jet.

After establishing the evidence for the existence of the away jet, one may review its characteristic features. In general, they are similar to those of the trigger jet.

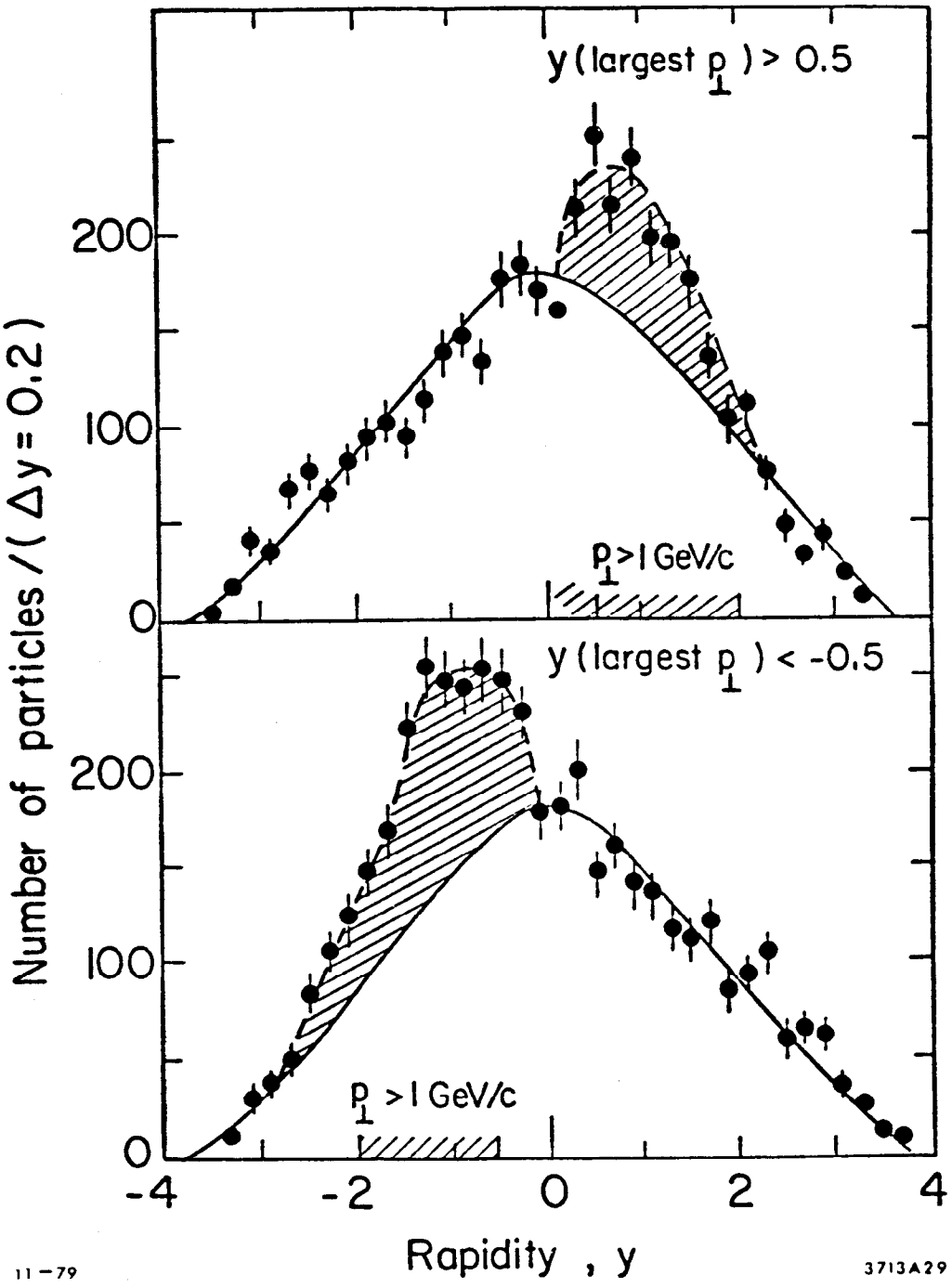

Fig. 28. Rapidity distribution for charged particles with p_T > 0.5 GeV/c on the away side when the "jet leader" is first seen with its rapidity in the shaded area (ref. 71).

i) The pattern of correlations shows presence of close pairs of large p_T particles. Both neutral and doubly charged configurations are present and the resonance production, although present, does not dominate.

ii) The distribution of particles inside the jet appears to be symmetric around the jet axis. The transverse momentum with respect to the jet axis is compatible with being gaussian with the average value of k_T in the range of $\langle k_T \rangle \sim 450 \div 600$ MeV/c.

iii) The average multiplicity of the particles in the jet is consistent with logarithmic increase with the jet momentum.

iv) The fragmentation of the jet is usually well described by an exponential function

$$\frac{dN}{dz} = Ae^{-Bz}$$

with the slope B independent of the trigger momentum (see Fig. 29). The value of the slope depends, however, on the type of experiment and method analysis and may be also energy dependent. It is found to be B = 4.6 in the FNAL jet experiment[72] and B = 7 at the ISR.[73] The ISR experiment of A^2BCS group has found also an evidence for the jet fragmentation into the single particle occurring at the level of about 1%. This observation may be interpreted both as the argument for the existence of the CIM terms and as the estimate of the size of their contribution to the away side jet. Such an estimate is nevertheless biased by the effects of the trigger on the towards side.

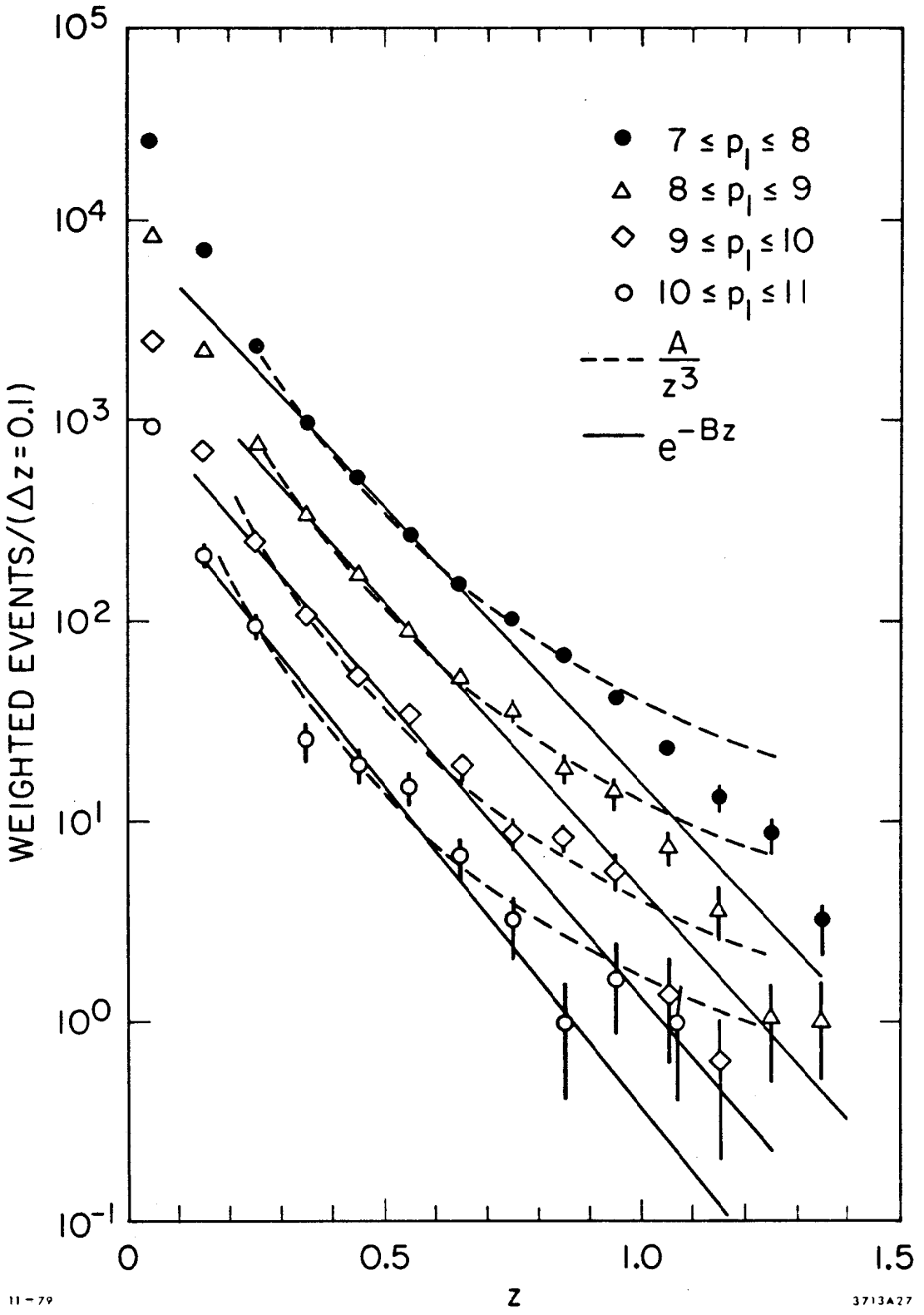

Fig. 29. The constituent fragmentation distribution into π^o measured by the A^2BCS Collaboration.

Several groups observed[74,75] a qualitative agreement of the global features of the away jet with those characterising jets measured in e^+e^- annihilations and deep inelastic lepton scattering. In large p_T processes substantial fraction of final state jets is expected to be due to gluon decay. In contrast, in e^+e^- annihilations and νp interactions, the final state jets are dominated by the fragmentation of quarks. The similarity of the various jets, if it is not accidental, i.e., if it does not result from the model dependent correction procedures applied during the analysis of the data, indicate that there is little qualitative difference between the quark and gluon jets. The experiments with much larger p_T of the triggers and cleaner separation of jets are needed for more quantitative study of this problem.

7.3 Correlations Among Jets

The measurements of the correlations among large p_T jets provide the unique opportunity to study the parton-parton interactions. The topical problems addressed most often during the past few years are the coplanarity and p_T balance of the jet, which are related to the transverse momentum of partons inside the colliding hadrons, and the quantum number correlations, which may be due to some higher order effects.

i) Coplanarity and p_T balance. In the absence of parton transverse momentum one expects coplanarity of the jets emerging from the 2→2 elementary subprocess. In addition, the two jets of fragments of scattered constituents should balance their overall transverse momentum. The first indication of the possible deviation from such picture was the observation

by the CCHK group[76] of the strong azimuthal correlations between the large p_T trigger and leading particles in the forward direction. In the extensive studies the British-French-Scandinavian Collaboration estimated[77] that the forward particles balance about 300 MeV/c of the trigger transverse momentum (see Fig. 30). Such value is compatible with expectations, discussed in Section 3, for the intrinsic parton k_T due to confinement.

The studies of the imbalance of the scattered jets yield, however, much greater values of k_T. At the ISR such conclusions follow from the measurents of p_{out}, the transverse momentum component out of the trigger plain. The distribution of p_{out} is found[64,69] to be gaussian with the average value depending on x_E and the trigger p_T. It is related to the intrinsic k_T by

$$\langle p_{out} \rangle = \sqrt{\langle q_T \rangle^2 + x_E(\langle q_T \rangle^2 + \langle k_T \rangle^2)} \quad ,$$

where q_T describes the transverse momentum in the fragmentation function. Several experiments obtained the values of $\langle k_T \rangle$ of the order of 1 GeV/c. In Figure 31 the two typical values of $\langle k_T \rangle$ extracted by the CERN-Saclay group[75] using two different methods are compared with the values measured by the Fermilab-Lehigh-Pennsylvania-Wisconsin two-jet experiment.[78] In general, they are compatible with the results of the analysis of massive lepton pair production and are larger than $\langle k_T \rangle$ = 848 MeV/c used in Feynman, Field and Fox

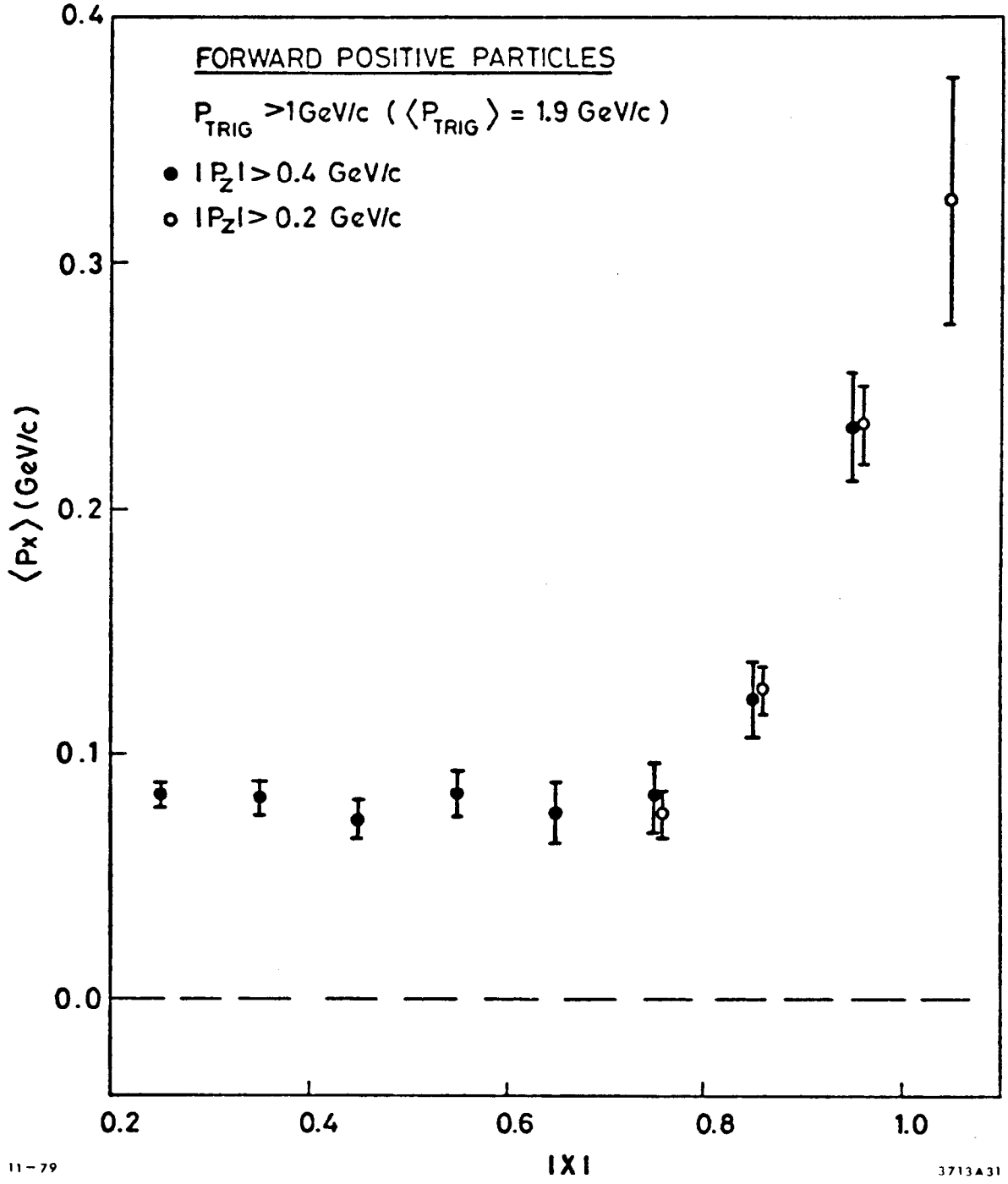

Fig. 30. The mean value of p_x for all positive particles versus x. Transverse momentum of the trigger is p_T > 1 GeV/c (ref. 77).

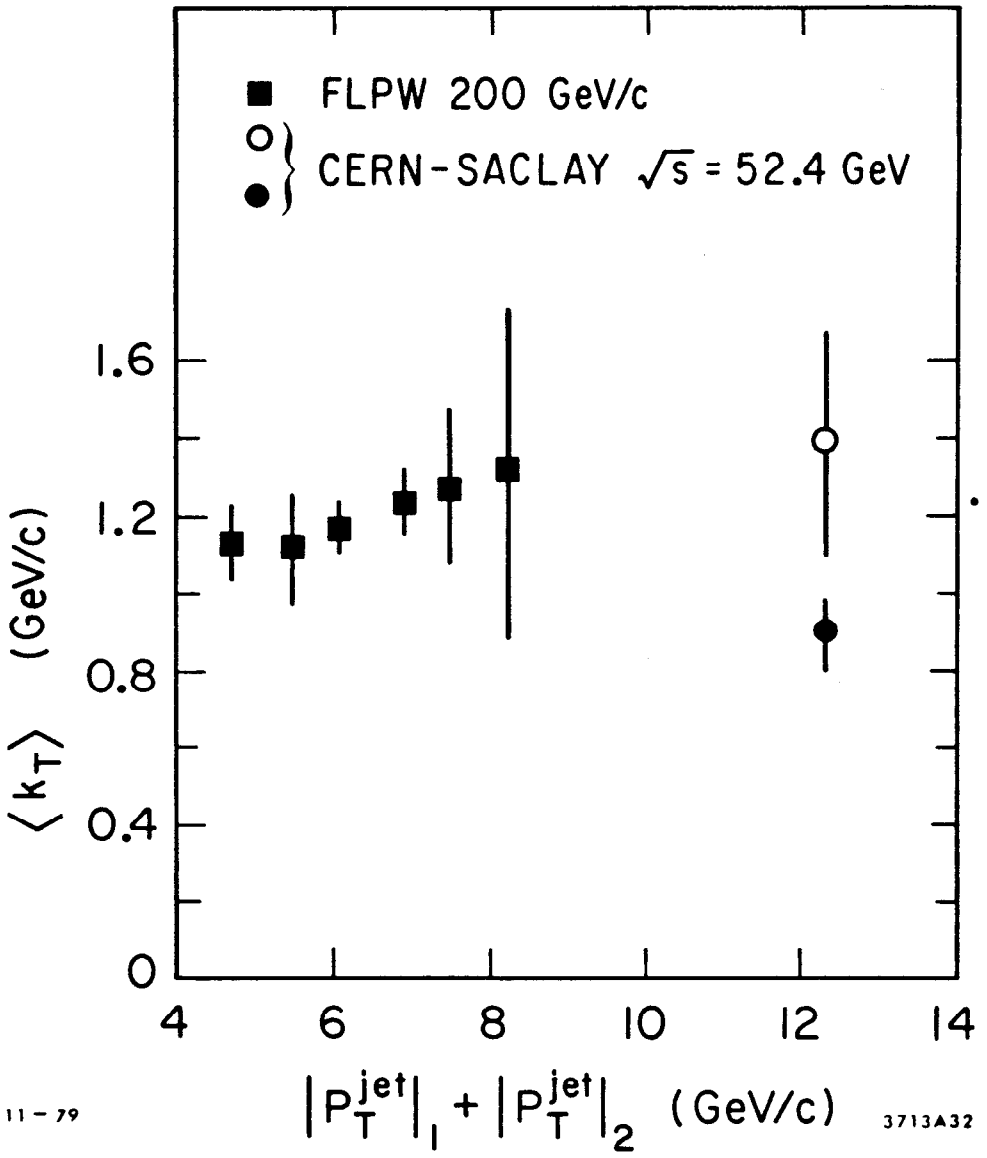

Fig. 31. Average transverse momentum with respect to the jet axis, $\langle k_T \rangle$, as function of total momentum carried by the two jets.

QCD phenomenology.[19] Part of this effect is probably due to the contribution of higher order processes not included so far in their approach.

ii) Quantum number correlations. In the simple gluon exchange parton model, the point-like scattering of constituents is independent of the quark flavour. Small charge correlations are predicted due to the different probabilities of finding the up and down quarks in a proton. These expectations are unchanged in the lowest order Quantum Chromodynamics. In contrast, higher order contributions, and in particular the CIM terms, may introduce substantial charge and flavour correlations.

In Fig. 32 are presented the data obtained by the British-French-Scandinavian Collaboration.[65] For the negative triggers (especially K^- and $\bar{p}$) the average number of positive particles on the away side is substantially higher than that of the negative particles. Similar effect, shown in Fig. 33, is observed in the recent Caltech-UCLA-FNAL-Illinois-Indiana experiment.[79] In both experiments the measured ratio is greater than expected from lowest order QCD calculations indicating the contributions of higher order terms.

8. OUTLOOK

Vast amount of data on large p_T processes is now available. Most of those data are described by the QCD phenomenology with impressive success.

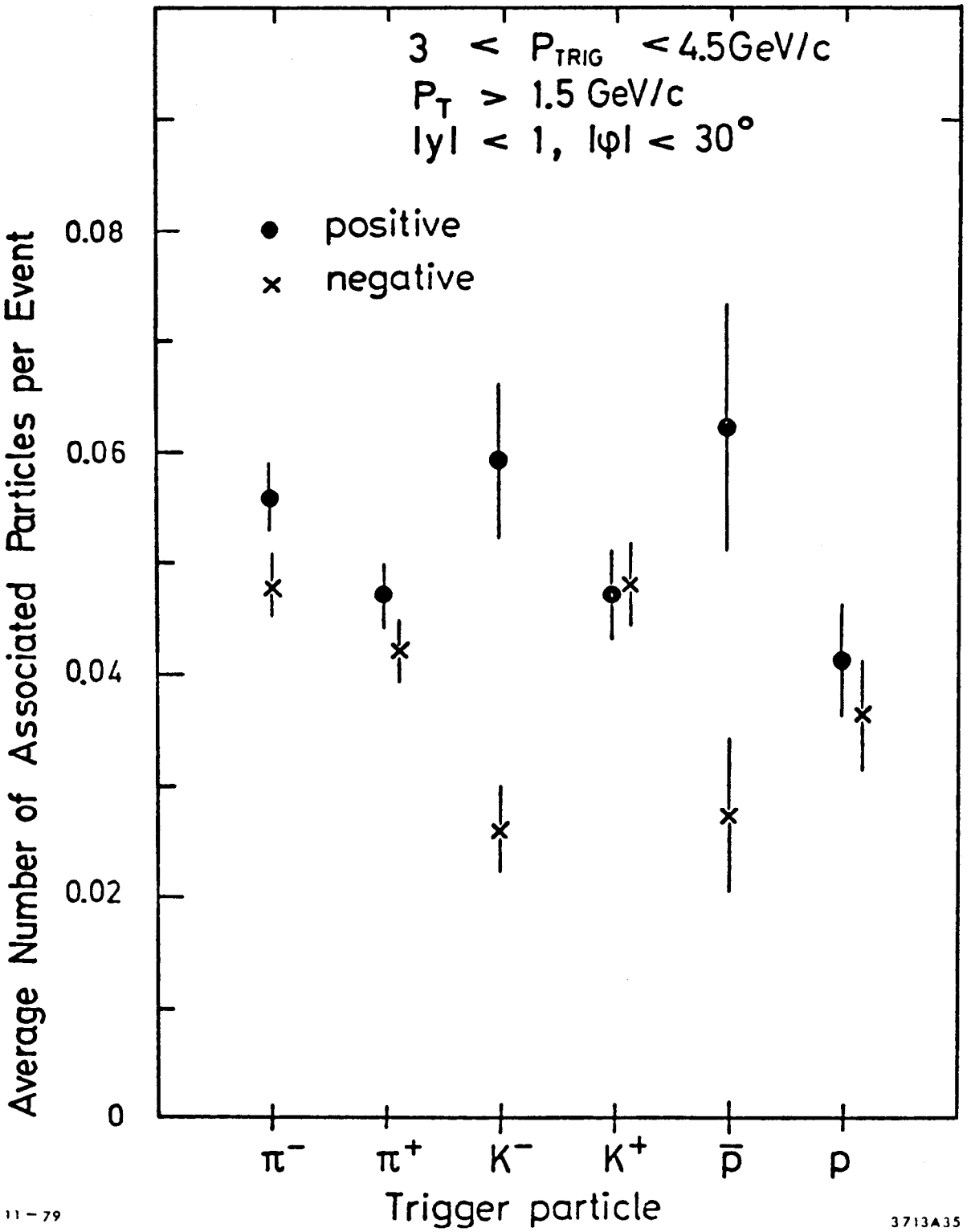

Fig.32. The average number of observed positive and negative particles with p_T > 1.5 GeV/c on the away side, associated with six different types of trigger particles (ref. 65).

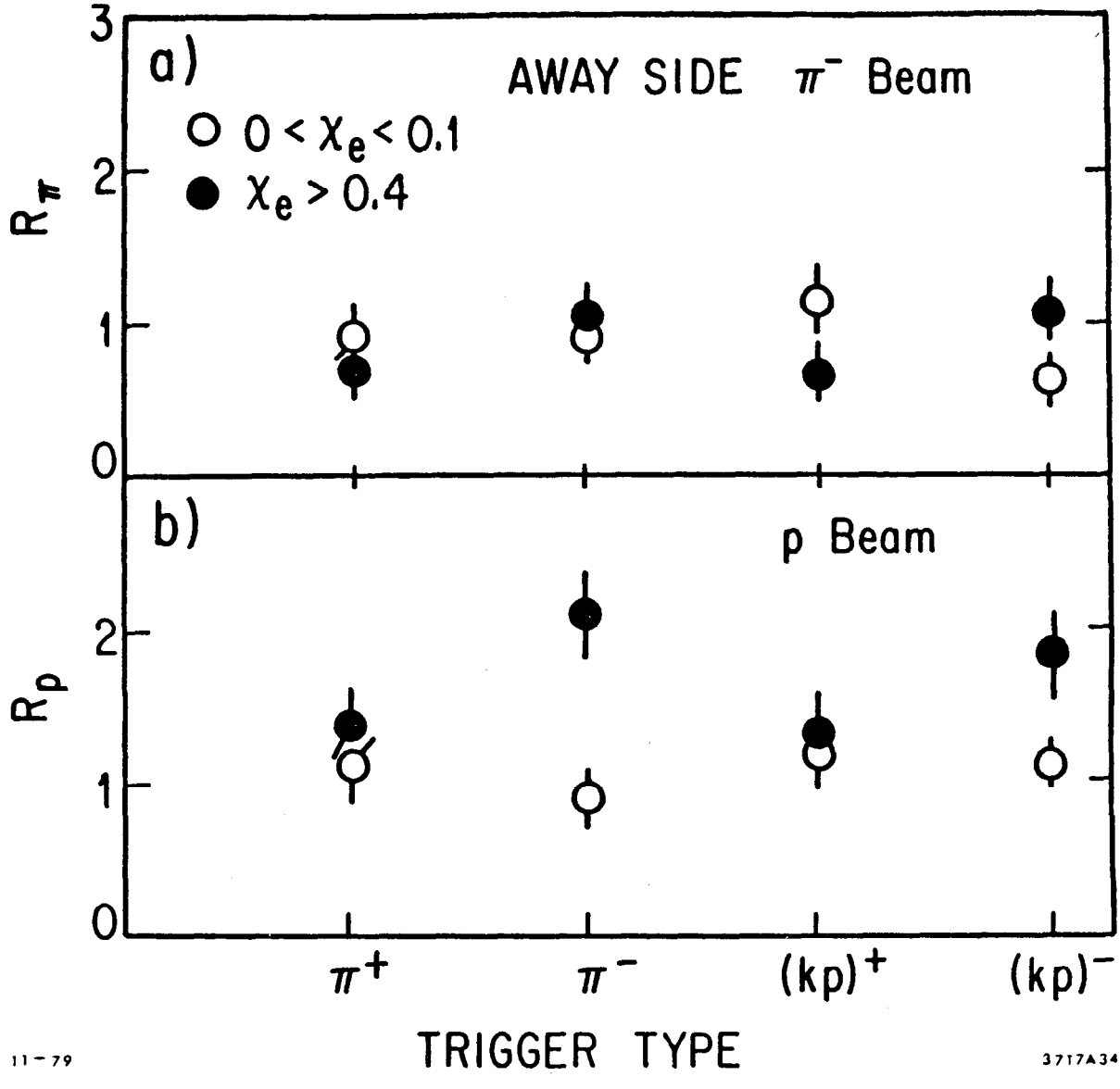

Fig. 33. The away side ratio of cross sections for production of positive and negative secondaries for various trigger particles (ref. 79).

Almost all results for $p_T < 10$ GeV/c may be understood by the mixture of the lowest order QCD subprocesses and some higher order effects. The latter are as yet not fully understood and are probably negligible at larger transverse momenta. Due to may terms and the complexity of calculations the field does not present any clean test of Quantum Chromodynamics. Nevertheless, it provides the unique opportunity to study parton-parton and possible parton-nucleon interactions. The experiments on heavy nuclear targets and at the future high energy machines will undoubtedly yield many interesting results.

ACKNOWLEDGMENTS

In the course of preparing these lectures I have profited greatly from many conversations with my colleagues at SLAC. I would like to thank D. Blockus, S. Brodsky, R. Field and F. Gilman for many clarifying discussions.

REFERENCES

1. B. Alper et al., Phys. Letters 44B, 521 (1973).
2. M. Banner et al., Phys. Letters 44B, 537 (1973).
3. F. W. Büsser et al., Phys. Letters 46B, 471 (1973).
4. S. M. Berman, J. D. Bjorken and J. B. Kogut, Phys. Rev. D4, 3388 (1971).
5. S. D. Ellis and M. B. Kislinger, Phys. Rev. D9, 2027 (1974).
6. D. Sivers, S. Brodsky and R. Blankenbecler, Phys. Reports C23, 1 (1976).
7. S. D. Ellis and R. Stroynowski, Rev. of Mod. Phys. 49, 753 (1977).
8. M. Jacob and P. V. Landshoff, Phys. Reports 48, 285 (1978).
9. S. J. Brodsky and G. Farrar, Phys. Rev. Letters 31, 1153 (1973).
10. V. Matveev, R. Muradyan and A. Tavkhelidze, Nuovo Cimento Letters 7, 719 (1973).
11. R. Blankenbecler and S. J. Brodsky, Phys. Rev. D10, 2973 (1974).
12. R. D. Field and R. P. Feynman, Phys. Rev. D15, 2590 (1977).
13. R. P. Feynman, R. D. Field and G. C. Fox, Nucl. Phys. B128, 1 (1977).
14. B. Blankenbecler, S. J. Brodsky and J. F. Gunion, Phys. Rev. D12, 3469 (1975).
15. P. V. Landshoff and J. C. Polkinghorne, Phys. Rev. D8, 4157 (1973).
16. R. Stroynowski, "Massive Lepton Pair Production," Lectures at this School, SLAC-PUB 2402.
17. H. D. Politzer, Nucl. Phys. B129, 301 (1977).
    C. T. Sachrajda, Phys. Letters 76B, 100 (1978).
    W. Furmanski, Phys. Letters 77B, 312 (1978).

18. B. L. Combridge, J. Kripfganz and J. Ranft, Phys. Letters 70B, 234 (1977).

R. Cutler and D. Sivers, Phys. Rev. D16, 679 (1977); Phys. Rev. D17, 196 (1978).

19. R. P. Feynman, R. D. Field and G. C. Fox, Phys. Rev. D18, 3320 (1978).

20. J. F. Owens, Phys. Rev. D20, 221 (1973) and Invited to talk at the Coral Gables Conference "Orbis Scientiae," January 1979. FSU-79214.

21. J. F. Owens, E. Reya and M. Gluck, Phys. Rev. D18, 1501 (1978).

22. D. Jones and J. F. Gunion, Phys. Rev. D19, 867 (1979).

23. S. J. Brodsky, Physica Scripta 19, 154 (1979).

24. R. D. Field, Lectures at the La Jolla Institute Summer Workshop, 1978, Caltech report CALT-68-696.

25. For the extensive discussion of the perturbative approach see S. Brodsky's lectures at this school.

26. A. P. Contogouris, S. Papadopoulos and M. Hongoh, Phys. Rev. D16, 2607 (1979).

27. F. Halzen, G. A. Ringland and R. G. Roberts, Phys. Rev. Letters 40, 991 (1978).

28. G. Altarelli and G. Parisi, Nucl. Phys. B126, 298 (1977).

29. D. J. Gross, Phys. Rev. Letters 32, 1071 (1974).

30. R. D. Field and R. P. Feynman, Nucl. Phys. B136, 1 (1978).

31. R. Blankenbecler, S. J. Brodsky and J. F. Gunion, Phys. Rev. D18, 900 (1978).

32. R. D. Field, Rapporteurs talk at the 19th International Conference on High Energy Physics, Tokyo, 1978.

33. W. E. Caswell, R. R. Horgan and S. J. Brodsky, Phys. Rev. D18, 2415 (1978); R. R. Horgan and P. Scharbach, Phys. Letters 81B, 215 (1979).

34. G. Altarelli, R. K. Ellis and G. Martinelli, Nucl. Phys. B157, 461 (1979).

35. F. W. Büsser et al., Nucl. Phys. B106, 1 (1976).

36. D. Antreasyan et al., Phys. Rev. D19, 764 (1979).

37. B. Alper et al., Nucl. Phys. B100, 237 (1975).

38. A.L.S. Angelis et al., Phys. Letters 79B, 505 (1978).

39. R. M. Baltrusaitis et al., "Inclusive π^o production over large x_T and x_F ranges in 200, 300 and 400 GeV/c proton-beryllium interactions," FERMILAB-PUB-79/37 (1979).

40. C. Kourkoumelis et al., Phys. Letters 84B, 271 (1979).

41. A. G. Clark et al., Phys. Letters 74B, 267 (1978).

42. F. W. Büsser et al., Phys. Letters 55B, 232 (1975).

43. C. Kourkoumelis et al., Phys. Letters 84B, 277 (1979).

44. G. J. Donaldson et al., Phys. Rev. Letters 40, 684 (1978).

45. H. Frisch, Contribution to the XIV Rencontre de Moriond, March 1979.

46. C. Bromberg et al., Phys. Rev. Letters 43, 565 (1979) and 43, 1058 (1979).

47. R. Rückl, S. J. Brodsky and J. F. Gunion, Phys. Rev. D18, 2469 (1978).

48. R. M. Baltrusaitis et al., FERMILAB preprint Pub-79/38 EXP (1979).

49. E. Amaldi et al., Nucl. Phys. B150, 326 (1979).

50. C. Bromberg et al., Phys. Rev. Letters 42, 1202 (1979).

51. G. Fox, Invited to talk at the APS Division of Particles and Fields Meeting, Argonne National Laboratory, 1977.

52. R. L. McCarthy et al., Phys. Rev. Letters 40, 213 (1978).

53. D. A. Finley et al., Phys. Rev. Letters 42, 1031 (1979).

54. K. W. Yung, Ph.D. thesis, California Institute of Technology, 1979.

55. J. H. Kühn, Phys. Rev. D13, 2948 (1976).

56. A. Bialas, Invited to talk at the IX International Symposium on Multiparticle Dynamics, Tabor, 1978.

57. A. Krzywicki et al., Phys. Letters 85B, 407 (1979).

58. A. Krzywicki and B. Petersson, Phys. Rev. D6, 924 (1972), J. Finkelstein and R. D. Peccei, Phys. Rev. D6, 2606 (1972), S. J. Brodsky and N. Weiss, Phys. Rev. D16, 2325 (1977).

59. J. Ellis, M. K. Gaillard and G. G. Ross, Nucl. Phys. B111, 253 (1976) and B130, 516 (1977).
G. Sterman and S. Weinberg, Phys. Rev. Letters 39, 1436 (1977).

60. J. D. Bjorken, Phys. Rev. D8, 4098 (1973) and Acta Physica Polon. B5, 893 (1974).

61. S. D. Ellis, M. Jacob and P. V. Landshoff, Nucl. Phys. B108, 93 (1976).

62. W. Selove, Talk given at the 14th Rencontre de Moriond, 1973, University of Pennsylvania preprint UPR-70E.

63. M. Jacob, Rapporteurs talk at the EPS International Conference, Geneva, 1979, CERN preprint TH 2700.

64. R. Sosnowski, Rapporteurs talk at the 19th International Conference on High Energy Physics, Tokyo, 1978.

65. M. G. Albrow et al., Nucl. Phys. B145, 305 (1978).

66. A.L.S. Angelis et al., Contribution to the 19th International Conference on High Energy Physics, Tokyo 1978.

67. H. Boggild, Contribution to the 14th Rencontre de Moriond, 1979, Niels Bohr Institute preprint NBI-HE-7-6.

68. A. G. Clark et al., "Experimental study of the fragmentation of large transverse momentum jets in high-energy p-p collisions," Contribution to the 19th International Conference on High Energy Physics, Tokyo, 1978.

69. M. J. Tannebaum, Talk at the 14th Rencontre de Moriond, 1979, Rockefeller University Report No. COO-2232A-79.

70. C. Kourkoumelis et al., Nucl. Phys. B158, 39 (1979).

71. M. Della Negra et al., Nucl. Phys. B127, 1 (1977).

72. C. Bromberg et al., Nucl. Phys. B134, 189 (1978).

73. C. Kourkoumelis et al., Phys. Letters 86B, 391 (1979).

74. M. G. Albrow et al., "Studies of proton-proton collisions at the CERN ISR with an identified charged hadron of high transverse momentum at 90°, III jet-like structures," CERN preprint EP/79-56 (1979) submitted to Nucl. Phys.

75. A. G. Clark et al., "Large transverse momentum jets in high-energy proton-proton collisions," CERN preprint EP/79-74 (1979) submitted to Nucl. Phys.

76. M. Della Negra et al., Phys. Letters 59B, 401 (1975).

77. M. G. Albrow et al., Nucl. Phys. B135, 461 (1978).

78. M. D. Corcoran et al., "Evidence that high p_T jet pairs give direct information on parton-parton scattering," University of Wisconsin preprint COO-088-105 (1979).

79. C. Bromberg et al., Phys. Rev. Letters 43, 561 (1979).

80. M. Diakonou et al., "Direct production of single photons at the CERN ISR," paper submitted to the EPS Conference on High Energy Physics, Geneva, 1979.